$\gamma\gamma$ Physics

Conveners: P. Aurenche, G.A. Schuler

Working group: A. Bawa, E. Boudinov, A. Buijs, M. Cacciari, A. Corsetti, W. Da Silva, M. Dubinin, R. Engel, F. Erné, J. Field, A. Finch, J. Forshaw, R. Godbole, J.Ph. Guillet, S.R. Hou, F. Kapusta, B. Kennedy, M.N. Kienzle, M. Krämer, P. Kroll, E. Laenen, M. Lehto, L. Lönnblad, D. Miller, G. Pancheri, J. Parisi, D. Perret-Gallix, J. Ranft, T. van Rhee, S. Riemersma, V. Serbo, M.H. Seymour, Y. Shimizu, T. Sjöstrand, S. Söldner-Rembold, M. Stratmann, I. Tyapkin, A. Vogt, J. Ward, B. Wilkens, A. Wright, N.I. Zimin

Contents

This chapter is devoted to QCD and, more generally, Strong Interaction studies in $\gamma\gamma$ collisions. For our purposes, LEP2 is a continous energy $\gamma\gamma$ collider with a reach of up to 100 GeV center of mass energy for some observables. At low energy, the main studies concern resonance production and quasi two-body processes which probe the meson and baryon wave-functions. At high energy, the partonic structure of the photon plays a dominant role and, as for hadronic processes, several tests of perturbative QCD, using many different observables, are possible. A specific feature of $\gamma\gamma$ collisions is the variability of the mass of the incoming photons which can be used to tune the non-perturbative component of the photon.

1 Introduction

While LEP1 was dedicated to the study of Z^0 production and decays the dominant process at LEP2 will be $e^+e^- \to e^+e^-X$ where the system X is produced in the scattering of two quasi-real photons by $\gamma\gamma \to X$. It is well known that[1] this cross section grows like $(\ln s/m^2_{electron})^2$, where s is the invariant energy squared of the incoming e^+e^- pair, whereas the annihilation cross section decreases like s^{-1}. Thus LEP2 can be considered as the highest luminosity as well as the highest energy $\gamma\gamma$ collider presently available. When one of the outgoing electrons is tagged it is possible to probe the photon "target" at short distance in deep-inelastic experiments. In fact, concerning the study of the hadronic structure of the photon (*i.e.* its quark and gluon content) LEP2 is the analogue of both an *ep* collider and *pp* collider for the study of the proton structure. As in the purely hadronic case the main processes of interest in this respect will be, besides deep-inelastic scattering, large p_T phenomena and heavy flavor production. The high luminosity (500 pb^{-1}) and the high energy (in the following we use $\sqrt{s} = 175$ GeV) available will make it possible to undertake precision phenomenology and obtain quantitative tests of perturbative QCD. Furthermore, combining LEP2 data with the lower energy TRISTAN and LEP1 data and with the high luminosity, high energy HERA results on photoproduction, a truly quantitative picture of the hadronic structure of the photon should emerge over a wide kinematical domain. Let us recall that a precise knowledge of the photon structure is required if reliable estimates are to be made of the background to new physics expected at LEP2.

Considering semi-inclusive or exclusive processes at high energy and relatively high momentum transfer it should be possible to probe diffractive phenomena and shed some light on the nature of the perturbative Pomeron (the so-called BFKL Pomeron) and the elusive Odderon (with vacuum quantum numbers but negative C-parity). These topics have undergone very interesting developments recently in connection with HERA results.

Finally, the traditional domain of $\gamma\gamma$ physics has been the formation of resonances and the study of two-body reactions of the type $\gamma\gamma \to$ meson-meson or $\gamma\gamma \to$ baryon-$\overline{\text{baryon}}$. In the first case resonances in the C= +1 state, not directly accessible in e^+e^- annihilation, are easily produced in a clean environment: heavy resonances like η_c and χ_c's are produced more aboundantly than in previous e^+e^- colliders. In the second case, the present situation is often

[1] taking into account the finite angular acceptance of any detector

unclear and the LEP2 results, at higher energy, will be helpful to distinguish between various models and hadron wave-functions.

One should point out interesting differences between LEP2, as a $\gamma\gamma$ collider, and a hadron-hadron collider. In particular, in the former case the initial energy is not fixed: this will turn out to be a major nuisance in the study of the deep-inelastic structure function of the photon but it could be an advantage in the study of the semi-inclusive channels (because it could help disentangle perturbative from non-perturbative effects). Furthermore, using the forward detectors of the LEP experiments one can vary the "mass^2" of the incoming virtual photons. This will be used to better constrain the non-perturbative component in the photon, which rapidly decreases with the photon virtuality, in the study of deep-inelastic, total cross section or large p_T processes, for example. More generally, it will help understand the transition from a non-perturbative to a perturbative regime in QCD studies.

On the theoretical side, considerable progress has been recently achieved on the various topics mentioned above. Of particular interest for data analysis and the study of the event structure of $\gamma\gamma$ collisions is the existence of several general purpose Monte-Carlo codes (ARIADNE, JETSET, HERWIG, PHOJET, PYTHIA) which are described in the "$\gamma\gamma$ event generator" chapter. These generators are adapted from hadron-hadron and electron-positron studies and they have been (or are being) tuned to HERA data thus incorporating all the physics constraints necessary to reliably describe $\gamma\gamma$ reactions. The crucial test of confronting in detail the models with the LEP1 results on $\gamma\gamma$ physics is still in progress as both data and models are very recent and little discussion on this point will be given below. In any case, the situation is much improved compared to only a year ago, when essentially every experimental group had its own specific event generator, making the comparison between the various experimental results rather delicate. One interesting outcome of the recent studies is that the global features of $\gamma\gamma$ scattering are predicted to be rather similar to those of hadron-hadron scattering at the same energy.

For the anticipated quantitative studies in perturbative QCD one obviously needs theoretical predictions at (at least) the next-to-leading logarithmic order in perturbation theory. All relevant calculations for $\gamma\gamma$ processes have been performed or are being completed. Depending on the channel under study it will be seen that the sensitivity of the theoretical predictions under the various unphysical parameters (scales) is not perfect but, overall, the situation is not worse than in the purely hadronic channels.

The plan of the chapter is as follows. We first discuss, in some detail, the deep-inelastic scattering process on a photon target ($\gamma^*\gamma$ process) and its relevance for the determination of the parton distributions and the Λ_{QCD} scale. We then turn to quasi-real $\gamma\gamma$ scattering and discuss the equivalent photon approximation, the (anti-)tagging conditions which define what we mean by $\gamma\gamma$ processes as well as the background to it. Global features of $\gamma\gamma$ events are described next. Large p_T phenomena and heavy flavor production are then discussed in the context of next-to-leading QCD phenomenology. The chapter ends with the discussion of resonance production and exclusive processes.

Photon-photon physics has been the object of many review articles, see *e.g.* [1, 2]. A look at [3] shows to what extent the scope of $\gamma\gamma$ physics has extended since the previous LEP2 workshop. The topics discussed below are described from a different perspective, and with complementary details, in the "$\gamma\gamma$ Event Generators" chapter [4].

2 Structure functions [2]

The measurements of the hadronic structure functions of the photon [5] at LEP1 and lower-energy e^+e^- colliders [6,7] can be extended in a number of important ways at LEP2. The higher beam energy will extend the kinematic reach both to lower Bjorken-x and to higher scales Q^2. Especially, the evolution of the real-photon structure function $F_2^\gamma(x, Q^2)$ can be investigated experimentally via single-tag events up to $Q^2 \approx 500$ GeV^2; and measurements can be done down to lower values of x than ever before, $x \approx 10^{-3}$, entering the small-x region where the HERA experiments observe a strong rise of the proton structure function F_2^p [8]. The increased integrated luminosity will be equally important, in principle allowing for a so far unachieved statistical accuracy of F_2^γ data of a few per cent over a large part of the accessible region. See sec. 2.1 for a more detailed discussion of the kinematical coverage, and sec. 2.3 for a study of the sensitivity of F_2^γ at LEP2 to the QCD scale parameter $\Lambda_{\rm QCD}$.

Improved techniques for reducing systematic uncertainties will be needed to exploit fully these increasing statistics and kinematical coverage, and to approach the experimental precision achieved in lepton-hadron structure function studies, cf. sec. 2.2 and the report of the "$\gamma\gamma$ event generator" working group in these proceedings. In this context, some of the experiments are improving tracking and calorimetry in the forward region to obtain a more complete coverage for $\gamma\gamma$ events, but no major detector upgrades are planned. Masking the detectors against the increased synchrotron radiation expected at LEP2 will limit the coverage of structure function measurements at low Q^2 to values above about 3 GeV^2.

There is no prospect of measuring the longitudinal structure function F_L^γ at LEP2. However, in sec. 2.4 a new technique is presented which could allow for a measurement of related unintegrated structure functions via azimuthal correlations between the tagged electron and an outgoing inclusive hadron or jet. Moreover, a sufficient number of double-tag events is expected at LEP2 for a study of the transition from quasi-real ($P^2 \ll \Lambda^2_{QCD}$) to highly-virtual ($P^2 \gg \Lambda^2_{QCD}$) photon structure. Although these measurements will remain limited by statistics at LEP2, they can considerably improve upon the present experimental information obtained by PLUTO [9] as discussed in sec. 2.5.

[2] J. Field, B. Kennedy, E. Laenen, M. Lehto, L. Lönnblad, D. Miller, G.A. Schuler, M.H. Seymour, M. Stratmann, I. Tyapkin, A. Vogt, J. Ward, A. Wright

2.1 Kinematical coverage for photon structure measurements

The kinematics of deep–inelastic lepton–photon scattering in e^+e^- collisions is recalled in Fig. 1a. Shown is the 'single–tag' situation, where the electron *or* the positron is detected at $\theta_{\rm tag} > \theta_0$, with a veto against a second tag anywhere in the detector. The bulk of the events useful for structure function studies are of this type; the generalization to 'double–tag' events is obvious. At LEP2, the limit of the main detector coverage will be about $\theta_0 \simeq 30$ mrad, slightly higher than at LEP1 due to the synchrotron radiation shielding already mentioned in the introduction. For double–tag events, the very forward calorimeters which are used for online high-rate luminosity monitoring will be employed (see sec. 2.5).

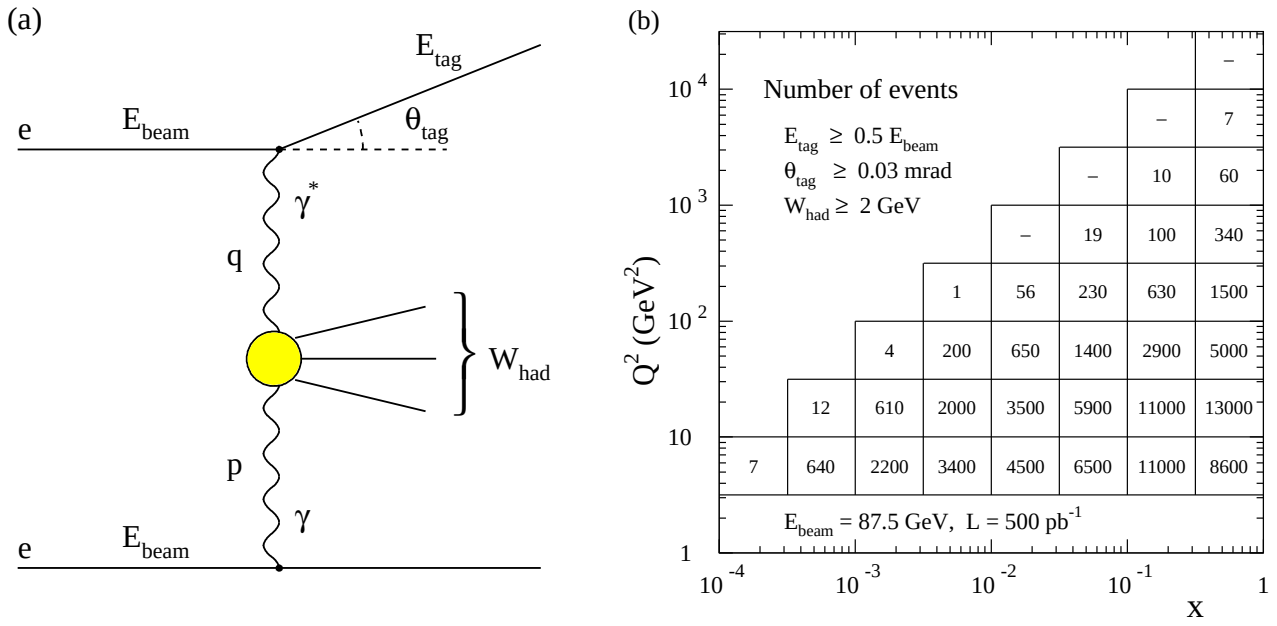

Figure 1: **(a)** *The kinematics of a single–tag inclusive $\gamma\gamma$ event.* **(b)** *The expected number of events for the determination of F_2^γ (including the charm contribution) at LEP2 (see text for details). The standard antitag Weizsäcker–Williams photon spectrum [10] has been used with $\theta < 30$ mrad. The LO GRV parametrization of the photon structure [11] has been employed to estimate F_2^γ.*

The cross section for (unpolarized) inclusive lepton–photon scattering reads to lowest order in the electromagnetic coupling α:

$$\frac{d\sigma(e\gamma \to eX)}{dE_{\rm tag}\, d\cos\theta_{\rm tag}} = \frac{4\pi\alpha^2 E_{\rm tag}}{Q^4 y}\left[\{1+(1-y)^2\}F_2^\gamma(x,Q^2) - y^2 F_L^\gamma(x,Q^2)\right] \ . \qquad (1)$$

Here $F_{2,L}^\gamma(x,Q^2)$ denote the structure functions of the real photon. The virtuality of the probing photon and the invariant mass of the (hadronic) final state are given by

$$Q^2 \equiv -q^2 = 2E_{\rm beam}E_{\rm tag}(1-\cos\theta_{\rm tag}) \ , \qquad W_{\rm had}^2 = (q+p)^2 \ , \qquad (2)$$

and we have introduced the usual dimensionless variables

$$x = \frac{Q^2}{Q^2 + W_{\rm had}^2} \ , \qquad y = 1 - \frac{E_{\rm tag}}{E_{\rm beam}} \cos^2\left(\frac{\theta_{\rm tag}}{2}\right) \ . \tag{3}$$

Since usually y^2 is rather small due to background suppression cuts, typically at least $E_{\rm tag} > 0.5\, E_{\rm beam}$, only F_2 has been accessible experimentally so far. Under these circumstances Q^2 is limited to the region $Q^2 > 3$ GeV^2 for $\theta_{\rm tag} \geq 30$ mrad at LEP2 energy, which in turn limits the reach towards small x.

It was demonstrated already at the 1986 LEP2 workshop [3] that the longitudinal structure function F_L would be very difficult to measure also at LEP2. This statement remains valid. Even in the most favoured kinematic region with $y > 0.5$, the correction from F_L to the main part of the signal due to F_2 is only about 14%. Achieving this marginal sensitivity in practice would require a costly (some 0.5 MChF per experiment) dedicated detector effort. The point is that events with $y > 0.5$ must have a low energy for the tagged electron. But experience at LEP1 has shown that there are significant numbers of off-momentum electrons that give spurious tags. To eliminate this background under present detector conditions, the so far published analyses for F_2 have required something like $E_{\rm tag} > 0.7\, E_{\rm beam}$ [6]. The off-momentum electrons come from beam–gas bremsstrahlung in the straight sections, and there is no reason to expect that their rate will be significantly reduced at LEP2.

The cross section (1) has to be convoluted with the Weizsäcker–Williams (WW) spectrum [10] for the photon, of virtuality P^2 (there is a high-P^2 tail which has to be corrected for in determinations of F_2^γ), emitted by the antitagged electron. For the explicit form of the WW spectrum see sec. 3. This fact leads to a key systematic problem in the determination of the photon structure functions: since p is unknown, $W_{\rm had}$ in eq. (2) and hence x in eq. (3) cannot by determined from the outgoing electron alone, in contrast to the situation in (electromagnetic) lepton–nucleon deep–inelastic scattering. This brings the hadronic final state into the game, of which only a part $W_{\rm vis}$ of the invariant mass is seen in the tracking regions of the detectors. The reconstruction $W_{\rm vis} \to W_{\rm had} \equiv W_{\rm true}$ requires a reliable modeling of the final state fragmentation. More on this issue can be found in sec. 2.2 and in the $\gamma\gamma$ event generator report.

Estimated event numbers for the measurement of $F_2^\gamma(x, Q^2)$, including the $\gamma^*\gamma \to c\bar{c}$ and $\gamma^* g \to c\bar{c}$ Bethe-Heitler charm contributions, are given in Fig. 1b in bins in x and Q^2. Only simple cuts have been applied here: on $E_{\rm tag}$, $\theta_{\rm tag}$ and $W_{\rm true}$. The nominal LEP2 integrated luminosity has been used[3]. Some $(0.5 \ldots 1) \cdot 10^6$ events, all in the deep–inelastic regime $Q^2 > 3$ GeV^2, can be expected, a dramatic increase over the rates that have been available for F_2^γ determinations so far [6, 7].

If we put aside the $W_{\rm vis}$ problem for a moment, and assume that a systematic error between 5% and 8% (depending on the statistical accuracy of the bin under consideration) can be

[3]The reduction in the event number due to further experimental final-state cuts ($W_{\rm vis}$ instead of $W_{\rm true}$, number of tracks etc.) will be approximately compensated by the presence of more than one experiment doing the measurements.

achieved, the potential of LEP2 on F_2^γ is illustrated in Fig. 2. Note that in regions where a high-precision measurement is statistically possible at LEP2, $Q^2 \lesssim 100$ GeV^2, such results will dominate our knowledge in the foreseeable future. A linear collider with 500 GeV center of mass energy is most likely to have no access to this region, since $\theta_{\rm tag}$ would be to small to be accessible there.

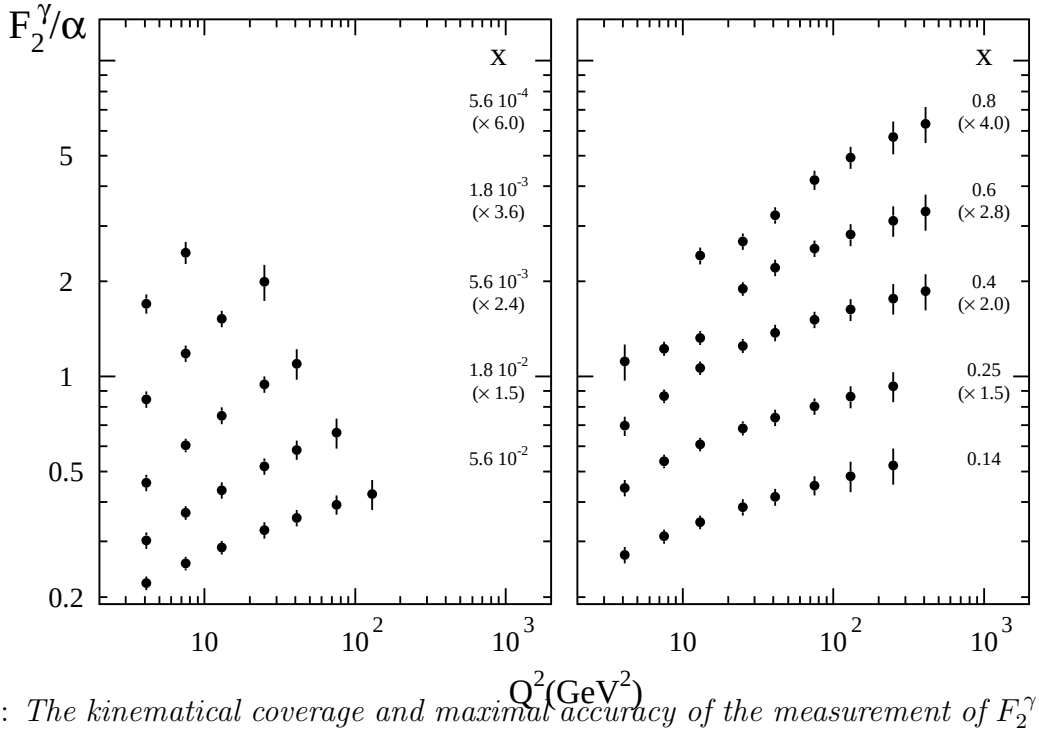

Figure 2: *The kinematical coverage and maximal accuracy of the measurement of F_2^γ at LEP2, using the event numbers of the previous figure for the statistical errors. The assumed systematic uncertainty of at least 5% has been added quadratically for the error bars shown. The central values have been estimated using the GRV(LO) parametrization [11].*

2.2 Determining F_2^γ from the experimental information

Unfolding the photon structure function at small x

The rise in the proton structure function F_2^p at small x [8] is one of the most important results reported from HERA so far. It has been suggested that this rise is a signal for so-called BFKL [12] evolution. However, the observed rise has been obtained from "conventional" Altarelli-Parisi renormalization group Q^2-evolution, by starting from a sufficiently low scale $Q_0^2 < 1$ GeV^2 [13], see also [14]. The small-x coverage of F_2^γ at LEP2 cannot compete with that of F_2^p at HERA, hence the LEP2 measurement cannot be expected to shed any new light on the origin of this rise. But an important check of the universality of the rise is possible, which will also provide valuable constraints on the parton densities of the photon at small-x, where they are dominated by their hadronic (vector meson dominance, VMD) component.

So far all measurements of F_2^γ have been at x-values above 0.01, which is outside the region where a rise would be expected. At LEP2, we expect to observe a significant number of events around and even below $x = 10^{-3}$ (see Fig. 1b), where a rise corresponding to that at HERA certainly should be visible. Measuring F_2^γ at such small x values is, however, far from trivial. While the value of Q^2 can be accurately determined to within a few per cent, since $\theta_{\rm tag}$ and $E_{\rm tag}$ are well measured, x is not directly measurable because the energy of the target photon is unknown. The conventional procedure has been to measure the visible hadronic mass $W_{\rm vis}$ in each event and calculate an $x_{\rm vis}$ using eq. (3). Then, an unfolding is made to get the true x distribution. This unfolding requires that the relationship between $W_{\rm vis}$ and $W_{\rm true}$ is well described by the event generator used.

During this workshop much work has been devoted to get a better understanding of how this unfolding behaves at small x. These results are described in more detail in the report from the "$\gamma\gamma$ event generator" working group in these proceedings. In that report methods to overcome these problems are also presented, using additional kinematic variables of the final state and limited information from the end-caps and the luminosity taggers, where much of the "missing" hadronic energy goes. The conclusion is that there is good hope that we will be able to measure at sufficiently small x to detect a rise in F_2^γ.

QED radiative corrections

In analogy to measuring F_2^p at HERA, an accurate measurement of F_2^γ must involve a careful treatment of radiative QED corrections to the basic one-photon exchange process described by eq. (1). Experiments have so far estimated the size of radiative corrections by comparing a Monte Carlo event generator for $e^+e^- \to e^+e^-\gamma\mu^+\mu^-$ [15] (with appropriate changes of the muon mass and charge to conform with $q\bar{q}$ production) to one for $e^+e^- \to e^+e^-q\bar{q}$ via $e\gamma \to eq\bar{q}$, with the photon energy distribution given by the Weizsäcker-Williams spectrum.

A more careful treatment would take into account the hadronic structure of the photon and effects of QCD evolution. Such a treatment is given in [16], in leading logarithmic approximation, which is known to be accurate to within a few percent for the proton case. It was found that the size of the corrections may vary from as much as 50% if one uses only so-called leptonic kinematic variables, to only a few per cent using only so-called hadronic variables. As the actual measurement will involve a mixture of such variables, a more extended study of the size of radiative corrections is needed.

2.3 The Q^2 evolution of F_2^γ and the QCD scale parameter Λ_{QCD}

At next-to-leading order (NLO) of the QCD improved parton model, the structure function $F_2^\gamma(x, Q^2)$ is related to the photon's parton distributions [5] via

$$\frac{1}{x}F_2^\gamma = \sum 2e_q^2\Big\{q^\gamma + \frac{\alpha_S}{2\pi}(C_q * q^\gamma + C_G * G^\gamma) + \frac{\alpha}{2\pi}e_q^2 C_\gamma\Big\} + \frac{1}{x}F_{2,h}^\gamma + \mathcal{O}\Big(1/Q^2\Big)\ , \qquad (4)$$

where $*$ denotes the Mellin convolution. The summation extends over the light u, d and s quarks. The heavy flavour contribution $F_{2,h}^{\gamma}$ has recently been calculated to second order in α_S [17] and is discussed in sec. 7. $C_{q,G}$ are the usual (scheme-dependent) hadronic NLO coefficient functions, and for the commonly used $\overline{\rm MS}$ factorization there is a 'direct' term $C_\gamma = 6\,C_G$. Besides the leading–twist contribution written out in (4), at large x (close to and within the resonance region) power-law corrections $\propto \mu^2/Q^2(1-x)$ become important, with μ being some hadronic scale. The Q^2-evolution of the quark and gluon densities q^γ, $G^\gamma(x,Q^2)$ is governed by generalized (inhomogeneous) Altarelli-Parisi evolution equations. For the singlet case the solution can be decomposed as

$$\vec{q}^{\,\gamma} = \begin{pmatrix} 2\sum_q q^\gamma \\ G^\gamma \end{pmatrix} = \vec{q}^{\,\gamma}_{PL} + \vec{q}^{\,\gamma}_{had} \ , \tag{5}$$

where the well-known homogeneous ('hadronic') solution $\vec{q}^{\,\gamma}_{had}$ contains the perturbatively uncalculable boundary conditions $\vec{q}^{\,\gamma}(Q_0^2)$. The photon-specific inhomogeneous ('pointlike', PL) part is given by

$$\vec{q}^{\,\gamma}_{PL} = \Big\{\frac{1}{\alpha_S} + \hat{U}\Big\} * \Big\{1 - [\alpha_S/\alpha_S(Q_0^2)]^{1+\hat{d}}\Big\} * \frac{1}{1+\hat{d}} * \vec{a} + \Big\{1 - [\alpha_S/\alpha_S(Q_0^2)]^{\hat{d}}\Big\} * \frac{1}{\hat{d}} * \vec{b} + \mathcal{O}(\alpha_S) \ . \tag{6}$$

Here $\vec{a}$, $\vec{b}$, $\hat{d}$ and $\hat{U}$ are combinations of the LO and NLO splitting-function matrices.

At asymptotically large Q^2 *and* large x, eq. (6) reduces to the well-known asymptotic solution $\propto 1/\alpha_S$, suggesting a parameter-free extraction of $\Lambda_{\rm QCD}$ from the photon structure. At energies accessible at present and in the foreseeable future, however, the non-asymptotic contributions cannot be neglected even at large x, and $\Lambda_{\rm QCD}$ determinations involve a model or a simultaneous free fit of the non-perturbative boundary conditions q^γ, $G^\gamma(Q_0^2)$. In eq. (6), Q_0^2 is an arbitrary reference scale; hence $\vec{q}^{\,\gamma}_{had}$ in eq. (5) will in general contain not only the non-perturbative (coherent) hadronic part, but also contributions originating in the pointlike photon–quark coupling. However, final state information suggests that there is some low scale Q_S^2 close to the border of the perturbative regime, where (in NLO in some suitable factorization scheme, see [18–20]) the parton structure of the photon is purely hadronic and given by the fluctuations to virtual vector mesons (VMD) [7, 21, 22].

In order to estimate the possible sensitivity of F_2^γ to $\Lambda_{\rm QCD}$ at LEP2, deep–inelastic electron–photon collisions corresponding to an integrated luminosity of $500\,{\rm pb}^{-1}$ have been generated using the SaS1D distribution functions [23], passed through a (fast) detector simulation (DELPHI) and unfolded using the Blobel program [24]. Possible systematic errors due to the dependence on fragmentation parameters have been neglected. We have chosen six bins in Q^2 (logarithmically distributed) and let the unfolding program choose the number and sizes of x bins. In total 21 bins have been obtained at $x > 0.1$, shown in Fig. 3. Alternatively, we have used the theoretical error estimates and bins of sec. 2.1 as representative for the best possible measurement using the combined statistics of two experiments.

Next, fictitious $F_2^\gamma(x,Q^2)$ data have been generated at these (x,Q^2) points. The input distributions of a simple toy-model have been evolved in NLO, which however yields very

similar numbers of events as the SaS [23] distributions. Thus the relative errors can be taken over from SaS. Specifically, the NLO parton distributions of the photon have been generated by a (coherent) sum of the three vector mesons ρ^0, ω, and ϕ at $Q_S = 0.6\,\mathrm{GeV}$ in the DIS_γ scheme [18].

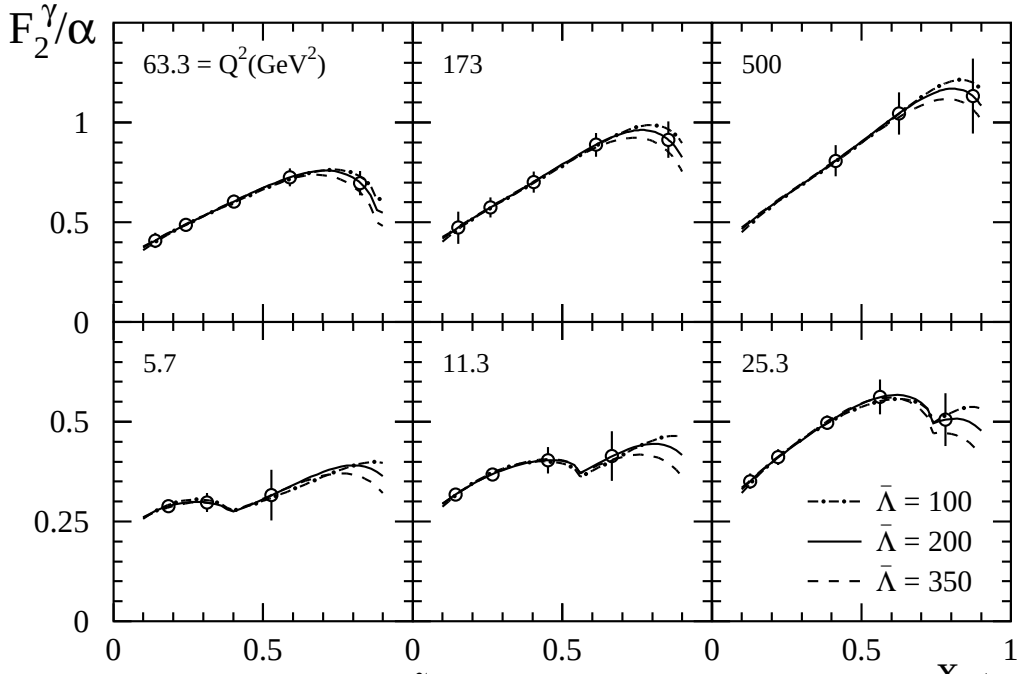

Figure 3: *The estimated accuracy of F_2^γ from one experiment at LEP2 using a (linear) Blobel unfolding [24]. The (in-)sensitivity to Λ_{QCD} is illustrated by the $\pm 1\sigma$ results described in the text. $\bar{\Lambda}$ denotes $\Lambda^{(4)}_{\overline{\mathrm{MS}}}$ in MeV.*

Finally, Λ_{QCD} is fitted together with the shape parameters N_s, a_i and b_i of the vector–meson valence, sea and gluon input distributions

$$xv(x) = \kappa N_v x^{a_v}(1-x)^{b_v}\ , \quad xS(x) = \kappa N_s x^{a_s}(1-x)^{b_s}\ , \quad xG(x) = \kappa N_g x^{a_g}(1-x)^{b_g} \tag{7}$$

at $Q_{\mathrm{ref}} = 2$ GeV (N_v and N_g are fixed by the charge and momentum sum rules of the vector mesons), the overall normalization κ, the scale Q_S, and the charm quark mass entering via $F^\gamma_{2,h}$ in eq. (4). The variation of the parameters is restricted to values reasonable for vector meson states, e.g., $0.8 \le b_v \le 1.3$ (the "data" were generated with the counting-rule value of 1.0). Using the Blobel-unfolded "results" of Fig. 3, one finds an experimental 1σ accuracy of

$$\Lambda^{(4)}_{\overline{\mathrm{MS}}} = \left(200^{+150}_{-100}\right)\ \mathrm{MeV} \quad \Rightarrow \quad \alpha_{\mathrm{s}}(\mathrm{M_Z}) = 0.109^{+0.010}_{-0.011}\ . \tag{8}$$

The sensitivity is dominated by the large-x region [25] as obvious from Fig. 3. If we use the "data" of sec. 2.1 instead, which need about the statistics of two experiments and some progress in the unfolding, especially at large x, we obtain

$$\Lambda^{(4)}_{\overline{\mathrm{MS}}} = \left(200^{+85}_{-65}\right)\ \mathrm{MeV} \quad \Rightarrow \quad \alpha_{\mathrm{s}}(\mathrm{M_Z}) = 0.109 \pm 0.006\ . \tag{9}$$

Hence, even under the most optimistic assumptions, the experimental error on $\Lambda_{\rm QCD}$ as determined from F_2^γ at LEP2 is a factor of two bigger than from fixed-target $ep\,/\mu p$ DIS. The theoretical scale–variation uncertainty of F_2^γ has been studied in [17] for fixed parton distributions. The resulting theoretical error on $\Lambda_{\rm QCD}$ is expected to be of similar size as in ep DIS. It should be mentioned that without the VMD-based restrictions on the parameter ranges the kinematical coverage and accuracy of LEP2 is not sufficient for any sensitive $\Lambda_{\rm QCD}$ determination.

2.4 Azimuthal correlations, a substitute for the longitudinal structure function

It has been mentioned already that F_L^γ will not be measurable at LEP2. However, F_L is not the only structure function that contains additional information. If, instead of just measuring the total cross-section $e\gamma \to eX$, one triggers on a final-state 'particle' a (either a hadron or a jet), more structure functions become accessible. The cross section as a function of the direction of a can be written in terms of the unintegrated structure functions $\widetilde{F}_P$, $P = T,\ L,\ A,$ and B, as

$$\frac{d\sigma(e\gamma \to eaX)}{dx\ dy\ d\Omega_a/4\pi} = \frac{2\pi\alpha^2}{Q^2}\frac{1+(1-y)^2}{xy}\Big[\Big(2x\widetilde{F}_T + \epsilon(y)\widetilde{F}_L\Big) - \rho(y)\widetilde{F}_A\cos\phi_a + \tfrac{1}{2}\epsilon(y)\widetilde{F}_B\cos 2\phi_a\Big]. \quad (10)$$

Here Ω_a represents the direction of a in the $\gamma\gamma^*$ rest-frame, and ϕ_a is its azimuth around the $\gamma\gamma^*$ axis, relative to the electron plane. The functions $\epsilon(y)$ and $\rho(y)$ are both $1+\mathcal{O}(y^2)$, and can be approximated by 1 throughout the accessible region of phase space. The standard structure functions F_2 and F_L are related to the corresponding $\widetilde{F}_P$ by integration over Ω_a.

For leptonic final states $\widetilde{F}_P$ are uniquely given by perturbation theory, while for hadronic final states these quantities involve a convolution over the parton densities of the photon:

$$\widetilde{F}_P(x,z) = \sum_{i=\gamma,q,g}\int_x^1 \frac{dx_p}{x_p}\ \frac{x}{x_p}f_{i/\gamma}\Big(\frac{x}{x_p}\Big)\ \widetilde{F}_P^i(x_p,z)\ , \quad (11)$$

where $f_{\gamma/\gamma}(x) = \delta(1-x)$ and $z = (p_a\cdot p_i)/(q\cdot p_i) = \frac{1}{2}(1+\beta\cos\theta)$, with β and θ denoting the velocity and direction of a in the $i\gamma^*$ rest-frame, respectively. One can find many incorrect formulae for $\widetilde{F}_P^i$ in the literature. We have performed an independent calculation and confirm the leading-order results given in [26], obtaining

$$\begin{aligned}
\widetilde{F}_T^\gamma(x_p,z) &= e_q^4\frac{\alpha}{2\pi}(x_p^2+(1-x_p)^2)\frac{z^2+(1-z)^2}{2z(1-z)} \\
\widetilde{F}_B^\gamma(x_p,z) = \widetilde{F}_L^\gamma(x_p,z) &= e_q^4\frac{4\alpha}{\pi}x_p^2(1-x_p) \\
\widetilde{F}_A^\gamma(x_p,z) &= e_q^4\frac{4\alpha}{\pi}x_p(1-2x_p)(1-2z)\sqrt{\frac{x_p(1-x_p)}{4z(1-z)}}
\end{aligned}$$

$$
\begin{aligned}
\widetilde{F}_P^g(x_p,z) &= \frac{T_R\alpha_s}{e_q^2\alpha}\widetilde{F}_P^\gamma, \qquad (12)\\
\widetilde{F}_T^q(x_p,z) &= e_q^2\frac{C_F\alpha_s}{4\pi}\left[\frac{x_p^2+z^2}{(1-x_p)(1-z)}+2(x_pz+1)\right]\\
\widetilde{F}_B^q(x_p,z) = \widetilde{F}_L^q(x_p,z) &= e_q^2\frac{2C_F\alpha_s}{\pi}x_p^2z\\
\widetilde{F}_A^q(x_p,z) &= e_q^2\frac{4C_F\alpha_s}{\pi}x_p(x_pz+(1-x_p)(1-z))\sqrt{\frac{x_pz}{4(1-x_p)(1-z)}}\ ,
\end{aligned}
$$

up to terms of order $m_q^2x/(1-x)Q^2$. In the quark case, the azimuth is that of the outgoing quark – the equivalent expressions for the outgoing gluon are identical but with z replaced by $1-z$ and $\widetilde{F}_A^q$ negated. The photon and gluon cases are identical for either outgoing parton.

Note that $\widetilde{F}_B^i = \widetilde{F}_L^i$ for all parton types, so a measurement of $\langle\cos 2\phi_a\rangle$ gives the same information about the parton content of the photon as F_L^γ, despite the fact that they arise from different spin states of the virtual photon (purely longitudinal for F_L and transverse-transverse interference for F_B).[4] This is a consequence of the fact that the struck parton is a fermion. In the leptonic case, the two outgoing particles can be distinguished, and the above distributions directly measured. In the hadronic case, however, quark, antiquark and gluon jets cannot be distinguished, and one must sum over all assignments. Since each event consists of two jets with z and $1-z$, all three sub-processes give equal and opposite $\cos\phi_a$-dependence for the two jets, and $\langle\cos\phi_a\rangle$ defined naively is identically zero. But if we instead use only the more forward of the two jets (i.e., the one with larger z, which is more often the quark in the $q\to qg$ case), the constant and $\cos 2\phi_a$ terms remain unchanged, but also the $\cos\phi_a$ term becomes nontrivial, being always negative for quarks and taking either sign for the other two processes, depending on x_p.

The measurement of azimuthal correlations involves reconstructing the hadronic final state to a much greater degree than does the measurement of the total cross-section. For this reason, a number of additional problems occur, including: How well do jet (or inclusive-particle) momenta mirror the underlying parton momenta? How well can the jets be reconstructed experimentally? How much are the azimuthal correlations smeared by the fact that the $\gamma\gamma^*$ rest-frame is not exactly known, or by target photon mass effects? How much artificial (de)correlation is induced by the fact that any cuts made in the lab frame are azimuth-dependent in the $\gamma\gamma^*$ rest-frame? A detailed detector-level study would be needed to answer these points, as discussed for CELLO in [27], but this has not yet been done for LEP2 energies. However, azimuthal correlations have been measured on a proton target at HERA [28], and in the leptonic final-state on a photon target at PETRA [29] and LEP1 [30], and all of the above problems have been addressed, and overcome, in one or other of these analyses. It thus seems hopeful that the measurement can be done at LEP2.

[4] In fact this has only been proved at lowest order. Different definitions of $\widetilde{F}_B$ (eg. single-particle vs. jet inclusive) will have different higher-order corrections, and it is currently unknown whether any obey the same relationship at higher orders.

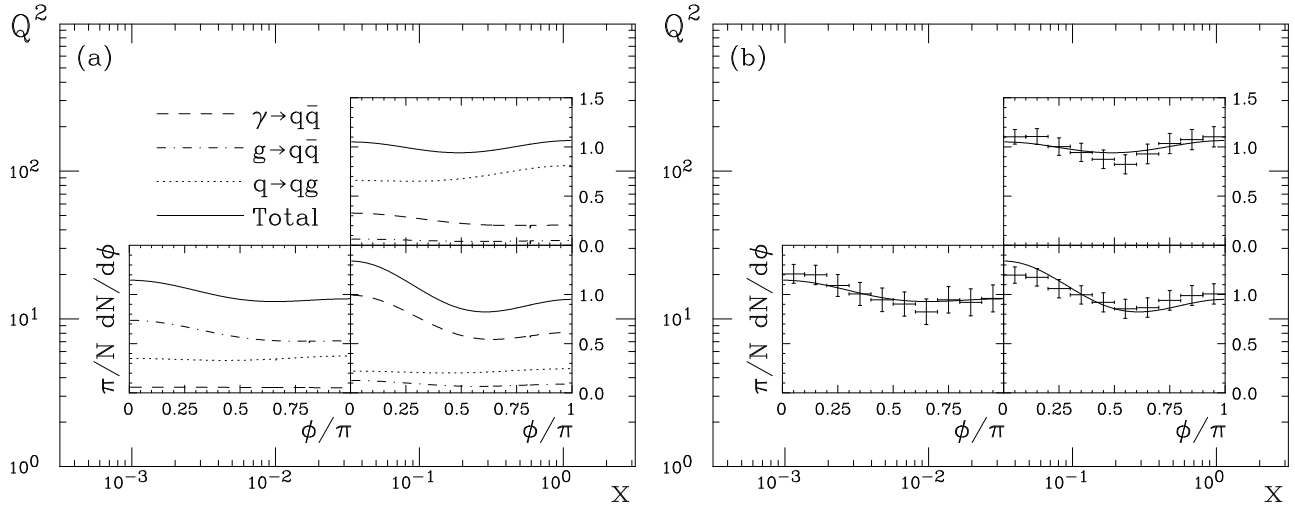

Figure 4: *Distribution of azimuthal angle of the more forward jet in two-jet events. Canonical cuts are made, plus a 2 GeV jet-p_t cut. In* **(a)** *parton–level results are shown,* **(b)** *depicts generator-level results (data points with statistical errors corresponding to 500 pb^{-1}), in comparison with the total parton-level prediction of (a).*

In the absence of a detailed experimental investigation, the group has performed a brief generator-level study using HERWIG, version 5.8d [31]. The jet reconstruction and cuts are loosely based on those used by the H1 collaboration [28], adapted for our assumed LEP2 detector coverage. The difficulties in measuring x discussed in the context of F_2 are left aside – it is assumed that x and Q^2 are perfectly known. Events passing the canonical cuts are selected ($E_{tag} > 0.5\,E_{\rm beam}$, $\theta_{tag} > 30\,$mrad and $W_{\rm vis} > 2\,$GeV within $|\cos\theta| < 0.97$). All particles within the central region are boosted to the Breit frame of the virtual photon and target electron beam[5], and jets are reconstructed using the $k_\perp$ jet algorithm [32], with a cutoff of 2 GeV. No attempt was made to optimize this value. As discussed in [33], the maximum correlations are achieved for $p_t = Q/2$.

In Fig. 4a we show parton-level results in three x and Q^2 bins, broken down into the contributions from the different parton types γ, q and g. By 'parton–level' we mean at leading order, with a direct correspondence made between partons and jets, and with the photon assumed collinear with the incoming electron beam. The SaS1D parametrization of $f_{i/\gamma}$ [23] has been used. We see that the $\cos 2\phi_a$-dependence arises predominantly from the gluon- and photon-induced sub-processes, and that a different initial-state parton dominates within each bin. In Fig. 4b generator-level results are presented, including parton showering, hadronization, jet reconstruction and target–mass smearing. The error bars shown correspond to the statistical errors one could expect from 500pb^{-1} of data. While the correlations are somewhat smeared, a signal still persists. It is possible that one could improve the statistics by including lower

[5]This frame has the same transverse boost as their rest-frame but a different longitudinal boost, which results in improved jet properties if a frame-dependent jet algorithm is used [32].

p_t scattering, provided a hadronic plane could be cleanly defined. Hence it seems likely that the azimuth–dependent structure functions of the photon can be measured at LEP2, providing additional constraints on the parton content of the photon.

2.5 Virtual photon structure

Effects of a non-zero virtuality of the target photon, $P^2 \neq 0$, have attracted considerable interest recently [23, 34–36]. The non-perturbative hadronic (VMD) contribution to the photon structure is expected to go away with increasing P^2, allowing for a purely perturbative prediction for $F_2^\gamma(x, Q^2; P^2)$ at sufficiently high P^2 [37]. The fall-off of the non-perturbative part with increasing P^2 is theoretically uncertain and model dependent [23, 36], hence experimental clarification is required. An improved understanding of this transition is also relevant for the experimental extraction of the real–photon structure functions, since corrections of the order of 10% have to be made to take into account the finite range of P^2 in single-tag events. However, the present experimental knowledge is very poor: the older[6] measurement of $F_2^\gamma(x, Q^2; P^2)$ by the PLUTO collaboration [9] suffers from low statistics and a rather limited kinematical coverage: $Q^2 = 5$ GeV^2, $P^2 \leq 0.8$ GeV^2, and $x \gtrsim 0.1$. Some new data are however being collected at HERA [38].

Especially because of its higher energy, but also due to its increased integrated luminosity, LEP2 can provide much improved information from double-tagged events. The rate of such events in the main forward luminometers ($\theta > 30$ mrad for the electron *and* the positron) is very small. The more important double-tagged results at LEP2 are expected to come from events with first tags in the main forward luminometers ($\theta_1 > 30$ mrad) and second tags in the very forward calorimeters which are used for online high-rate luminosity monitoring in each of the four LEP experiments. These small detectors (currently being upgraded in ALEPH and L3) are situated at 7 – 8 meters from the interaction point, beyond the minibeta quadrupole magnets. The defocussing effect of the quadrupoles distorts the acceptance of the detectors, but lepton tags can be reconstructed in the range $5 \lesssim \theta_2 \lesssim 15$ mrad, yielding $0.1 \lesssim P^2 \lesssim 1.0$ GeV^2 (the exact coverage varies between experiments).

For 500 pb^{-1} of data collected at LEP2, it is expected that about 800 double-tagged events of this type will be seen within the range $3 \times 10^{-4} < x < 1$ and $3 < Q^2 < 1000$ GeV^2. The invariant mass of each event can be reconstructed from the two tagged leptons and hence the correlation between the measured value ($W_{\rm vis}$) and the true value is good – there is no loss of correlation at high W (unlike for single–tagged events, see sec. 2.2), and the structure function can be measured more easily down to low x.

Fig. 5 shows the virtual photon structure function $F_2^\gamma(x, Q^2; P^2)$ as predicted by the SaS1D, SaS2D [23] and GRS [36] models in two bins for P^2 and Q^2. The error bars indicate the statistical error expected on each point for a bin width leading to two points per decade in x, using the SaS1D parton distributions [23]. The SaS2D [23] and GRS [36] distributions, both

[6] Note that actually $F_{eff} \equiv F_2 + 3F_L/2$ was measured by PLUTO.

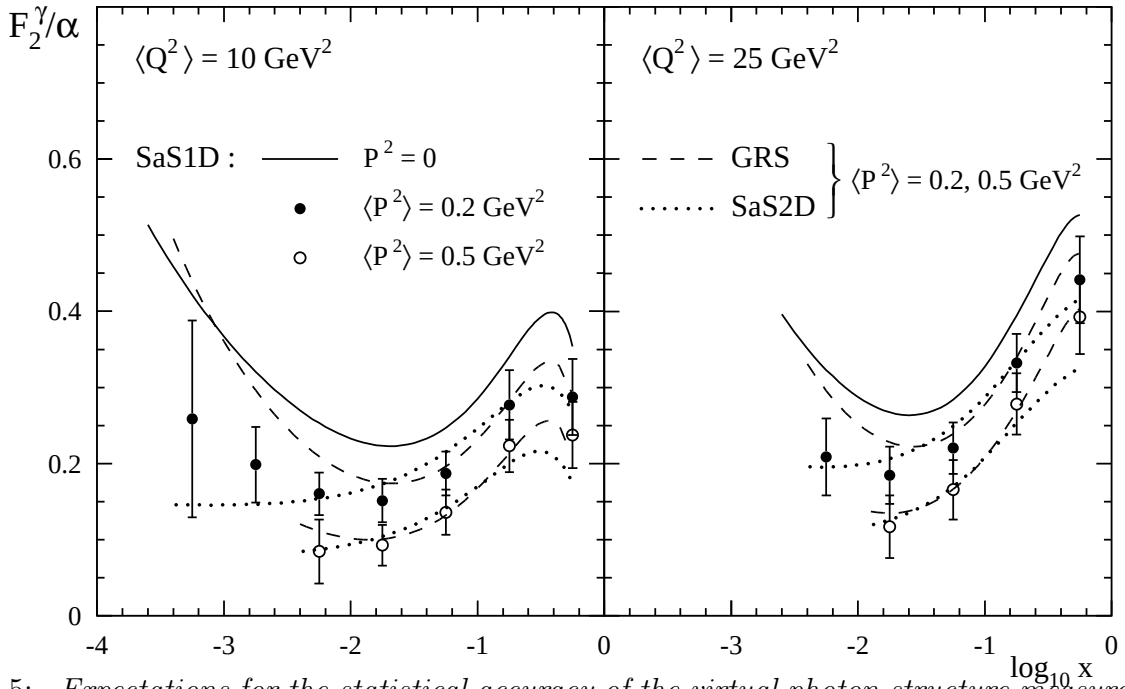

Figure 5: *Expectations for the statistical accuracy of the virtual photon structure measurement at LEP2 in two different P^2 and Q^2 bins, using the SaS1D [23] distributions. The SaS1D prediction for the real photon and the $P^2 \neq 0$ results for the GRS [36] and SaS2D [23] distributions are shown as lines for comparison. The upper (lower) curves for GRS and SaS2D refer to $P^2 = 0.2$ (0.5) GeV^2, respectively.*

showing a rather different small-x behaviour as compared to SaS1D, lead to similar results for the expected statistical errors. A measurement of $F_2^\gamma(x, Q^2; P^2)$, as distinct from the real ($P^2 = 0$) photon structure function (shown as solid curves for SaS1D), should be possible at LEP2 and could be compared to the results from PLUTO [9] in the region of overlap, as well as to different model predictions [23, 36]. Additional information will be obtained in single tag events where high p_T jets are produced (see sec. 6).

2.6 Summary

Due to its high beam energy and increased integrated luminosity, LEP2 will be a unique place for studying the hadronic structure functions of the photon. Some $(0.5 \ldots 1) \cdot 10^6$ single–tag events for deep–inelastic ($Q^2 > 3$ GeV^2) electron–photon scattering can be expected, for the first time allowing for a determination of F_2^γ (and hence of the photon's quark content) with statistically high precision up to scales Q^2 of a few 100 GeV^2 and down to Bjorken-x values as low as about 10^{-3}. Depending on how well systematic uncertainties can be controlled, a determination of the QCD scale $\Lambda_{\rm QCD}$ may become possible from F_2^γ. But even under optimistic assumptions, the experimental error on $\alpha_s(M_Z)$ will be about a factor of two bigger than that one obtained from electron–nucleon deep–inelastic scattering. It seems likely that supplementary information on

the parton densities can be obtained by measuring azimuthal correlations between the tagged electron and a final state hadron or jet. About 10^3 double–tag events are expected to be seen with $0.1 \lesssim P^2 \lesssim 1.0$ GeV^2 and Q^2 as above, allowing for a study of the virtual photon structure function over a much wider kinematical range than so far. It should be noted that the data taken at LEP2 on photon structure functions will dominate our knowledge in most of the accessible range discussed above for the foreseeable future, since a 500 GeV linear collider will most likely have no access to $Q^2 < 100$ GeV^2.

3 The equivalent photon approximation

The cross section for a $\gamma\gamma$ process is related to the cross section at the e^+e^- level, which is measured in the laboratory, by the formula

$$d\sigma(e^+e^- \to e^+e^- X) = \sigma(\gamma_1\gamma_2 \to X)\frac{d^2n_1}{dz_1 dP_1^2}\frac{d^2n_2}{dz_2 dP_2^2}dz_1 dz_2 dP_1^2 dP_2^2 \tag{13}$$

where z_i is the scaled photon energy in the laboratory frame and P_i^2 is the photon invariant mass. This is the equivalent photon approximation (EPA) [39] where the longitudinal polarization component as well as the mass of the incoming photons are neglected in $\sigma(\gamma\gamma \to X)$. The P_i^2 integration can be carried out to give the photon "density" in the $e^\pm$ (the photon flux) [10]

$$f_{\gamma/e}(z, P_{min}, P_{max}) = \int_{P_{min}^2}^{P_{max}^2} \frac{d^2n}{dz dP^2}dP^2 = \frac{\alpha}{2\pi}\left[\frac{1+(1-z)^2}{z}\ln\frac{P_{max}^2}{P_{min}^2} - 2m_e^2 z\left(\frac{1}{P_{min}^2} - \frac{1}{P_{max}^2}\right)\right]. \tag{14}$$

For untagged experiments P_{min} is the kinematic limit

$$P_{min}^2 = \frac{m_e^2 z^2}{1-z} \tag{15}$$

and $P_{max} \simeq E_{beam}$. The quality of the approximation is not guaranteed in this case as the EPA is derived under the hypothesis that $P^2 \ll E_{beam}^2$ which is not always satisfied here. In most of the following we use antitagging conditions where the $e^\pm$ are confined to small angles $\theta < \theta_{max}$ (typically $\theta_{max} = 30$ mrad) so that

$$P_{max}^2 = (1-z)E_{beam}^2\theta_{max}^2. \tag{16}$$

Using antitagging conditions rather than untagged conditions reduces somewhat the cross sections (about 30 % in the case of heavy flavor production and a factor 2 for large p_T jet production) but improves the reliability of the theoretical calculations based on the EPA. Finally for tagged conditions both P_{min}^2 and P_{max}^2 are set by the detector configuration.

Even in the case of antitagging it is always worthwhile, whenever possible, to check the validity of the EPA for each of the considered process. For large p_T jets and heavy flavor production a possible check consists in comparing, with the appropriate choice of cuts and

kinematics, the lowest order matrix element calculation of $e^+e^- \to e^+e^- q\bar{q}$ to the approximate one. Good agreement is found provided the "constant" (non-logarithmic) term is kept in eq. (14). If the constant term is ignored the cross sections are over-estimated by roughly 10% when both e^+ and e^- are antitagged. The same is true for minimum bias type physics. Special attention should be given to processes which involve the photon structure function, *i. e.*, the so-called resolved processes. Under certain conditions it may be necesary to take into account the effect of the virtuality of the quasi-real photons initiating the process. Indeed as written in eq. (5) the structure function has two components

$$F_{i/\gamma}(x, Q^2; P^2) = F^{PL}_{i/\gamma}(x, Q^2; P^2) + F^{had}_{i/\gamma}(x, Q^2; P^2) \tag{17}$$

with a different dependence in P^2, the virtuality of the quasi-real photon. In particular $F^{had}_{i/\gamma}$ is roughly suppressed by the usual VMD form factor $(m_\rho^2/(m_\rho^2 + P^2))^2$. In the tagged case ($P^2 \simeq .5$ GeV^2) or in the case with relatively large antitagging angles this factor should be taken into account when carrying out the integration over the virtuality in eq. (14). The result is a relative reduction of the "*had*" component of the photon compared to the case when the photon is assumed to be real. This reduction obviously affects the rate of the observable cross section. If the aim is to obtain predictions at a 10% accuracy this effect should certainly be studied in further details.

Turning now to resonance production (see sec. 8), eq. (13) simplifies since one of the z_i integration can be performed with the constraint $z_1 z_2 = \tau = M^2/s_{e^+e^-}$ where M is the resonance mass. It is then customary to define luminosity functions (see *e.g.* [40])

$$\frac{d\mathcal{L}}{dM} = \frac{2\tau}{M} \int dz_1 dz_2 f_{\gamma/e}(z_1) f_{\gamma/e}(z_2) \delta(z_1 z_2 - \tau) \tag{18}$$

so that

$$d\sigma(e^+e^- \to e^+e^- X) = \int dM \frac{d\mathcal{L}}{dM} \sigma(\gamma\gamma \to X). \tag{19}$$

This luminosity curve makes it easy, in principle, to determine the counting rate for resonance production knowing the width of the resonance in the $\gamma\gamma$ channel. An important point however concerns the acceptance cuts of the detector which reduce the observed rates compared to the theoretical predictions. Such cuts are taken into account in sec. 8. Detailed studies of luminosity curves were done for the previous LEP2 and we do not repeat them here [3].

4 Tagging conditions, cuts and background to $\gamma\gamma$ processes [7]

In this section we discuss what we call $\gamma\gamma$ events (as opposed to $\gamma^*\gamma$) *i.e.* events where the electron and positron of the diagram in Fig. 1 escape detection (*i.e.* essentially "go down the beam pipe"). This require a precise definition of the tagging conditions as well as the cuts necessary to reduce the background to $\gamma\gamma$ physics. Background sources come from all processes

[7] P. Aurenche, J.Ph. Guillet, F. Kapusta, D. Perret-Gallix, N.I. Zimin

not initiated by $\gamma\gamma$ interactions but exhibiting similar features such that they can be taken, mistakingly, for genuine $\gamma\gamma$ events. Background events are, essentially, of two types (Fig. 6).

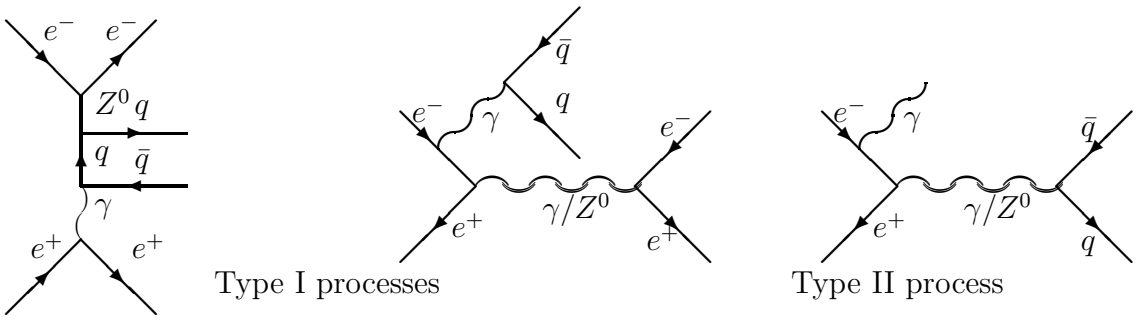

Type I processes Type II process

Figure 6: *Two types of background processes for $\gamma\gamma$ physics*

Type I events have similar final states, although being produced by different processes: for example, the t-channel γZ exchange diagram or the initial state photon splitting in a $q\bar{q}$ pair. The final state is therefore two electrons and a $q\bar{q}$ pair as in the signal. Type II background processes can arise from detector acceptance and resolution when some particles are lost down the beam pipe or in detector cracks or are misidentified. In this category, one can mention s-channel initial state radiation: when the photon is lost in the beam pipe and the boosted $q\bar{q}$ pair detected, this event can be interpreted as a no tag or antitag $\gamma\gamma$ event. Four fermions channels where two of the fermions are lost in the beam pipe region are also part of this category of $\gamma\gamma$ no tag events. A series of dedicated cuts based on kinematic constraints must be set to reject most of the background (largest purity), although keeping most of the signal (largest efficiency).

The LEP2 total cross sections are orders of magnitude smaller than those found at the Z^0 peak. However, initial state radiations by emitting a high energy photon, can shift down the centre of mass energy to the Z^0 peak energy. In the following we concentrate on the study of this background as the Type I backgrounds can be argued away easily: the γZ exchange processes are suppressed due to the Z propagator while the other process leads typically to a very small hadronic mass at large rapidity and leptons at large angle (which would be detected) or a large missing energy.

4.1 Tagging conditions and acceptances

Typical detector acceptances and thresholds have been selected in order to match an "average" LEP experiment. All momenta and angles are expressed in the laboratory frame. The events are selected by antitagging in the following way: both scattered electrons or photons have a polar angle $\theta \leq 30$ mrad or an energy $E \leq 1$ GeV. We define now the acceptance cuts on the final state particle system

cut 0: no further constraint applied to the final state with the exception of the electron or photon tagging conditions.

cut 1: Only charged particles with $20^\circ \leq \theta \leq 160^\circ$, $p > 0.4$ GeV/c and neutral particles with $10^\circ \leq \theta \leq 170^\circ$, $E > 1$ GeV are accepted for the analysis. At least four charged particles have to survive the cuts mentioned above to accept the event.

The visible energy is calculated from the invariant mass of the four-momentum obtained by summing the four-momenta of all particles satisfying cut 1. For jet search, a cone algorithm with a cone radius $R = \sqrt{(\Delta\eta)^2 + (\Delta\phi)^2} = 1$ has been used. Only particles passing cut 1 enter the jet analysis.

4.2 Radiative return to the Z^0 cross-section

Background simulation have been performed at $\sqrt{s} = 175$ GeV using JETSET 7.4 [41]. We

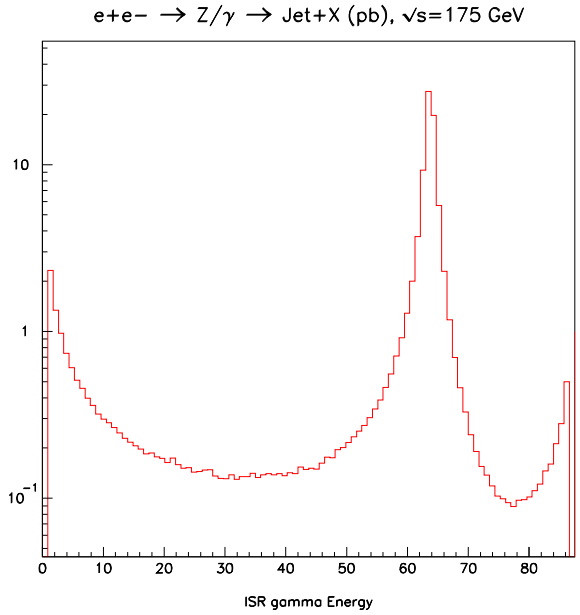

Figure 7: *Initial state radiated photon energy.*

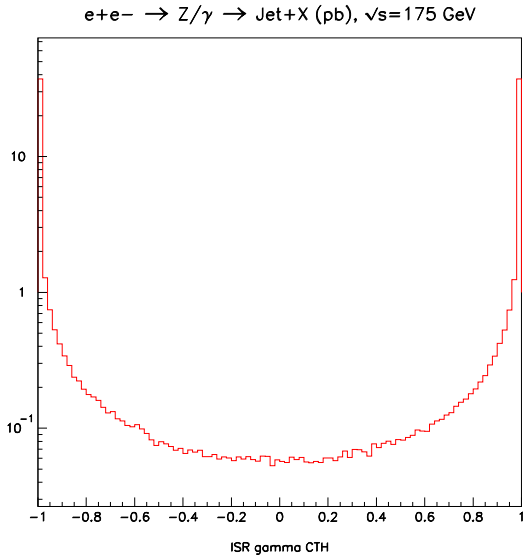

Figure 8: $\cos\theta$ *distribution of initial state radiation photon.*

show in Fig. 7 the initial state radiated photon energy. The low energy peak reflects the $1/E_\gamma$ behaviour of the bremsstrahlung process, the high energy peak comes from the $\sigma_o(\hat{s}) \propto 1/\hat{s}$ ($\hat{s} = (1-x_\gamma)s$) singularity of the Born term as found in the hard radiative cross-section formula:

$$\frac{d\sigma}{dx_\gamma} = \frac{\alpha_{em}}{\pi}(\ln\frac{s}{m_e^2} - 1)\frac{1+(1-x_\gamma)^2}{x_\gamma}\sigma_0(\hat{s}) \tag{20}$$

where x_γ is the fraction of the beam energy carried by the real photon and $\hat{s}$ is the invariant mass squared of the virtual photon. The large peak, close to 64 GeV, is precisely due to the so-called return to the Z^0 for $E_\gamma = (s - M_Z^2)/2\sqrt{s}$. The $\cos\theta$ distribution of the photon is shown in Fig. 8 where the forward and backward peaks reflect the cross section divergence for collinear photon production. If such a photon remains undetected, the boosted $q\bar{q}$ pair system may appear as a untagged $\gamma\gamma$ event. Even worse, the photon can be identified as an electron in the forward tagging detectors, this event would then be selected as a one tag $\gamma\gamma$ process.

The next three figures display clearly the differences between the signal and the radiative Z^0 production background. In these studies the charged hadrons angular acceptance has been

increased to 10^0 with a realistic track reconstruction efficiency as expected in DELPHI. The two-photon events are generated with TWOGAM and are compared to PYTHIA Zγ and $W^+W^- \rightarrow$ all decays production contributions allowing initial state radiation. As expected the signal is characterised by a rapidly falling $W_{\rm vis}$ distribution (due to the Weiszäcker-Williams convolution) while the background exhibits a clear peak slightly below the Z^0 mass and the W^+W^- channel shows up at very large invariant mass. Similarly the $\vec{P}_{\perp}^{vis}$, $\vec{P}_{\parallel}^{vis}$ spectra from the signal are confined to low values while they have a long tail for the background (figs. 9, 10). The above

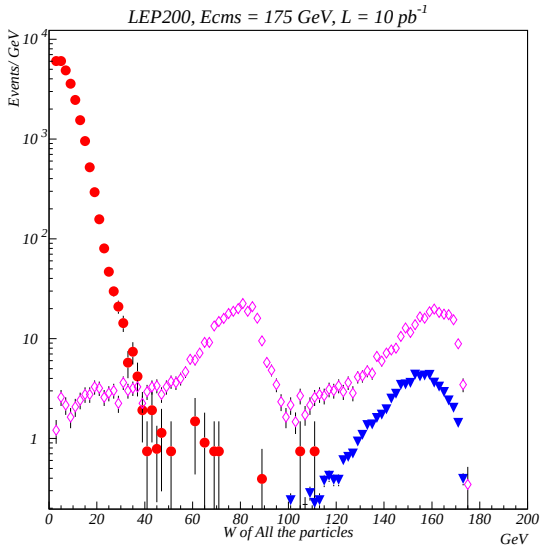

Figure 9: *Visible invariant mass of $\gamma\gamma$(solid dots), Zγ(open diamonds) and W^+W^-(solid triangles).*

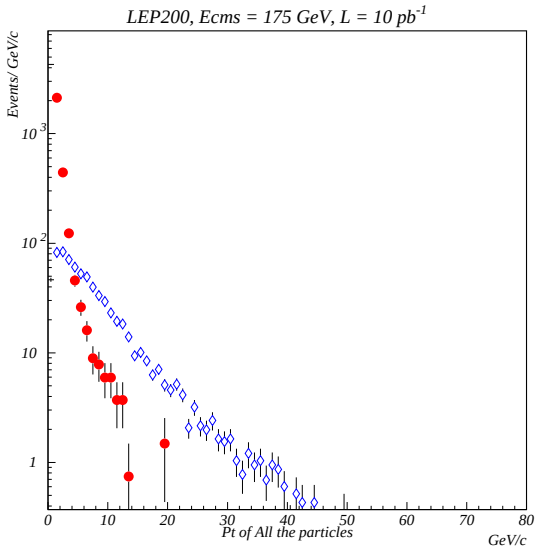

Figure 10: *$\vec{P}_{\perp}^{vis}$ distributions for the signal and the background. The symbols have the same meaning as in the previous figure.*

features clearly dictate the following cuts to reject the background still retaining most of the genuine $\gamma\gamma$ events:

cut 2: the vector sum of the transverse momenta of all accepted particles satisfies $\vec{P}_{\perp}^{vis} = \sum \vec{p}_{\perp} \leq 10$ GeV/c.

cut 3: the vector sum of the longitudinal momenta of all accepted particles satisfies $\vec{P}_{\parallel}^{vis} = \sum \vec{p}_{\parallel} \leq 20$ GeV/c.

cut 4: the invariant mass calculated from the four momenta of accepted particles satisfies $W_{\rm vis} \leq 50$ GeV.

Clearly these cuts will not affect the bulk of the $\gamma\gamma$ events (*e.g.* the total charm production cross section is hardly affected), however they will certainly reduce the rate of rare events in the signal characterized by a large invariant mass: this is the case of large p_T jet production since one has in general $W \geq 2p_T$. This is illustrated in Fig. 12 where the effect of the cuts on jet searches is discussed. Histograms represent the contribution of the Z^0 return background. The upper line is for events satisfying cut 1 above, the next lower ones are for cut 1+2, cut 1+2+3 and cut 1+2+3+4 respectively. The solid lines are the results of an analytic calculation in the leading-logarithm approximation at the partonic level where the cuts are approximately

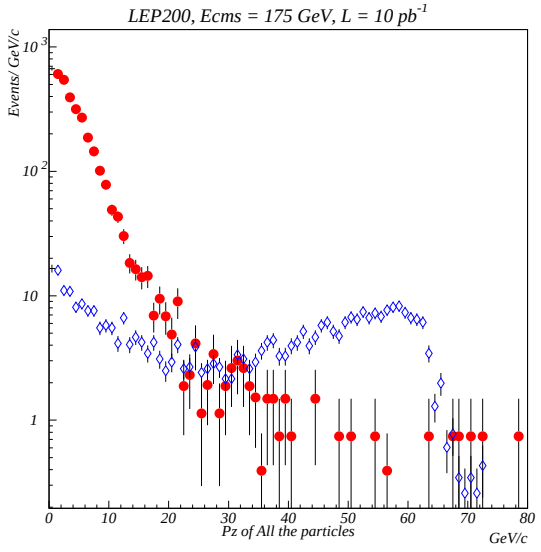

Figure 11: $\vec{P}_{\parallel}^{vis}$ *distributions for the signal and the background.*

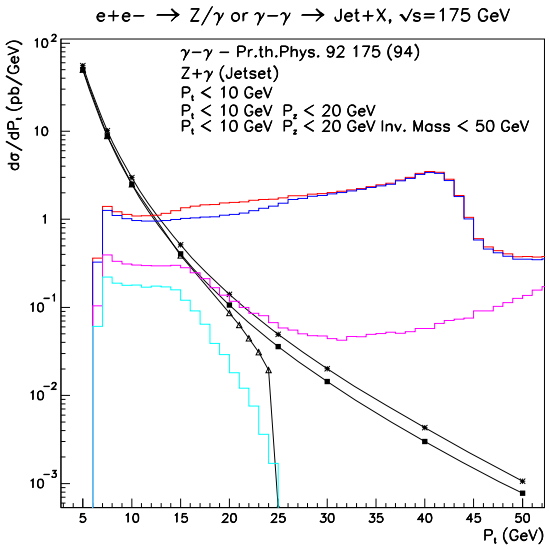

Figure 12: *Signal and background p_T distribution for various cuts. The cross section is integrated over the jet rapidity range $|\eta| = 1$. See the text for explanations.*

implemented: the top curve is for cut 1+2 (cut 2 is ineffective since $\vec{P}_{\perp}^{vis} = 0$ by definition) and the lower two curves are as above. The p_T threshold above which the background rate is larger than the signal rate goes from 13 GeV ($\vec{P}_{\perp}^{vis}$ cut) up to 16 GeV ($\vec{P}_{\perp}^{vis}$ and $\vec{P}_{\parallel}^{vis}$). The final visible invariant mass cut has a strong effect on the background but reject also most of the signal over $p_T > 20 - 25$ GeV. A more detailed study of the effects of the cuts on the signal is discussed in the "Large-p_T processes" section.

5 Soft and semihard physics, and event structure [8]

Studies of minimum-bias physics and semihard interactions in two-photon events offer a good opportunity to investigate the high-energy behaviour of scattering amplitudes and the transition from perturbative to non-perturbative QCD.

5.1 Cross section predictions and general characteristics

The photon, in its high-energy interactions with hadrons, behaves very much like a hadron, however with cross sections reduced strongly relative to pure hadronic cross sections. Simi-

[8] A . Corsetti, R. Engel, F. Erné, A. Finch, J. Field, J. Forshaw, R. Godbole, F. Kapusta, G. Pancheri, J. Ranft, G.A. Schuler, V. Serbo, T. Sjöstrand, N.I. Zimin

larly to a hadron, the photon both undergoes soft hadronic interactions and has resolved hard interaction between its hadronic constituents and the hadronic constituents of the target. Additionally, the photon has a direct pointlike interaction with the hadronic constituents of the target.

Even at high energies, many features of hadronic interactions of photons are dominated by soft multiparticle production. Correspondingly, distributions measured in photoproduction are similar to those obtained in purely hadronic interactions (provided, of course, these are taken at the same center-of-mass energy). This is nicely illustrated in Fig. 13 for the central transverse

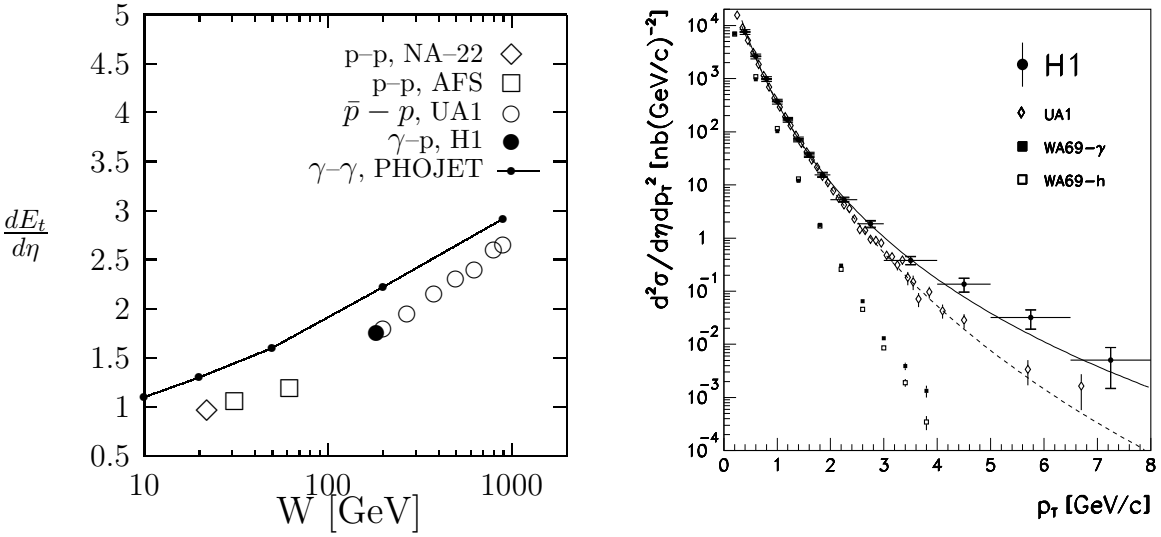

Figure 13: *(a,left) The transverse energy (in GeV) per unit of pseudorapidity in the central region (i.e. at $\eta = 0$) as a function of the hadronic CM energy W. Data from photoproduction are compared with data from hadron-hadron collisions; from [42]. For $\gamma\gamma$ collisions the* PHOJET *predictions are shown. (b right) Charged hadron differential cross sections for photon-hadron scattering compared to the shape of hadron-hadron scattering: the γp data from H1 at $\sqrt{s}$ = 200 GeV exceed in the high $p_\perp$ region the $\bar{p}p$ data from UA1 at the same energy. The results from a fixed target experiment (WA69) at $\sqrt{s}$ = 18 GeV show a similar difference between γp and hadron-hadron data; from [43].*

energy density and the one-particle inclusive p_T spectrum. It is only at high p_T that photon-induced reactions differ because of the photon's pointlike interactions and its correspondingly harder parton distribution functions (PDF). Based on these observations we can safely predict that minimum-bias physics of $\gamma\gamma$ interactions will follow that of γp or pp interactions. At high p_T, the spectra should become harder when going from pp to γp to $\gamma\gamma$ interactions.

In view of what we said above, any model that aims at an complete description of $\gamma\gamma$ interactions should better successfully describe the wealth of data taken in hadronic collisions, notably at $p\bar{p}$ colliders. Reactions to be modelled include elastic scattering, diffractive dissociation and hard, perturbatively calculable interactions. On top of that, unitarity constraints have to be incorporated implying, in general, the existence of multiple (soft and hard) interactions (for a review and references see e.g. [44]). The SaS model (Schuler and Sjöstrand) [45] has

been implemented in PYTHIA [41] while the DPM (Dual-Parton-Model) [46] has been extended (Engel and Ranft) to γp [47] and $\gamma\gamma$ reactions [48] in PHOJET. Minimum-bias physics in pp, γp, and $\gamma\gamma$ collisions is currently being improved in HERWIG by the inclusion of multiple hard scatterings [49].

These event generators and the physics of the corresponding models are described in detail in the "Event generators" chapter. Here we discuss only some differences among the three models which have been used in Fig. 14.

To extend the description of pp interactions to γp (and $\gamma\gamma$) ones it is convenient to represent the physical photon as the superposition [50]

$$|\gamma\rangle = \sqrt{Z_3}\,|\gamma_B\rangle + P^{\gamma}_{had}\,|\gamma_{had}\rangle \equiv \sqrt{Z_3}\,|\gamma_B\rangle + \frac{e}{f_{low}}\,|q\bar{q}_{low}\rangle + \frac{e}{f_{high}}\,|q\bar{q}_{high}\rangle\ , \tag{21}$$

where the (properly normalized) first term describes the pointlike interaction of the photon. The spectrum of hadronic fluctuations of the photon is split into a low- and a high-mass part, separated by some scale Q_0. Both contributions can, in general, undergo soft and hard interactions. The soft interactions are mediated by Pomeron/Reggeon exchange whose amplitudes can be inferred from the ones of pp interactions assuming photon–hadron duality. Hard interactions are those that contain at least one hard scale and can be expressed in terms of the "minijet" cross section $\sigma_{jet}(s; p_{Tmin})$, i.e. the cross section for perturbatively calculated partonic $2 \to 2$ scatterings above a p_T cutoff p_{Tmin}. Again, unitarization leads to multiple (soft and hard) scatterings.

In a most naïve scenario, the probability $P^{\gamma}_{had} = P(\gamma \to q\bar{q})$ is taken to be constant. At high energies, this cannot, however, be correct [50] since the contribution from high-mass hadronic fluctuations becomes important. These are perturbatively calculable and lead to a logarithmic increase of P^{γ}_{had} with the hard scale $Q \sim p_T$, $(e/f_{high})^2 \propto \ln(Q^2/Q_0^2)$. In the SaS approach [51], most parameters, in particular the coupling of the low-mass part of (21) are determined using VMD-type arguments. The only two additional parameters in the extension from pp to γp collisions, namely Q_0 and the p_T cutoff for the hard cross section originating from the high-mass part (p^{anom}_{Tmin}) were fixed by low-energy γp data, prior to the HERA data. Elastic and diffractive cross sections as well as minimum-bias distributions were succesfully predicted [44]. The prediction for the $\gamma\gamma$ total cross section is shown in Fig. 14.

The DPM approach extended to γp collisions [47] (in the PHOJET event generator) differs in several important aspects from the SaS approach. The unitarization requirements are obeyed by strictly sticking to the eikonal approach. This leads to[9] multiple partonic scatterings also for high-mass photonic states. Furthermore the probabilities e^2/f^2_{low} and e^2/f^2_{high} as well as the Pomeron and Reggeon coupling constants and effective intercepts have been determined by fits to data on the total photoproduction cross section and the cross section for quasi-elastic ρ^0 production. Once these parameters are fixed, $\gamma\gamma$ collisions can be predicted without further new parameters [48]. The predicted rise of $\sigma^{\gamma\gamma}_{tot}$ is shown in Fig. 14. It is governed by the small-x behaviour of the PDF of the photon.

[9] This also leads to another difference compared to PYTHIA, which is already present for purely hadronic collisions, namely the generation of events containing multiple soft interactions in combination with any number (including zero) of hard interactions.

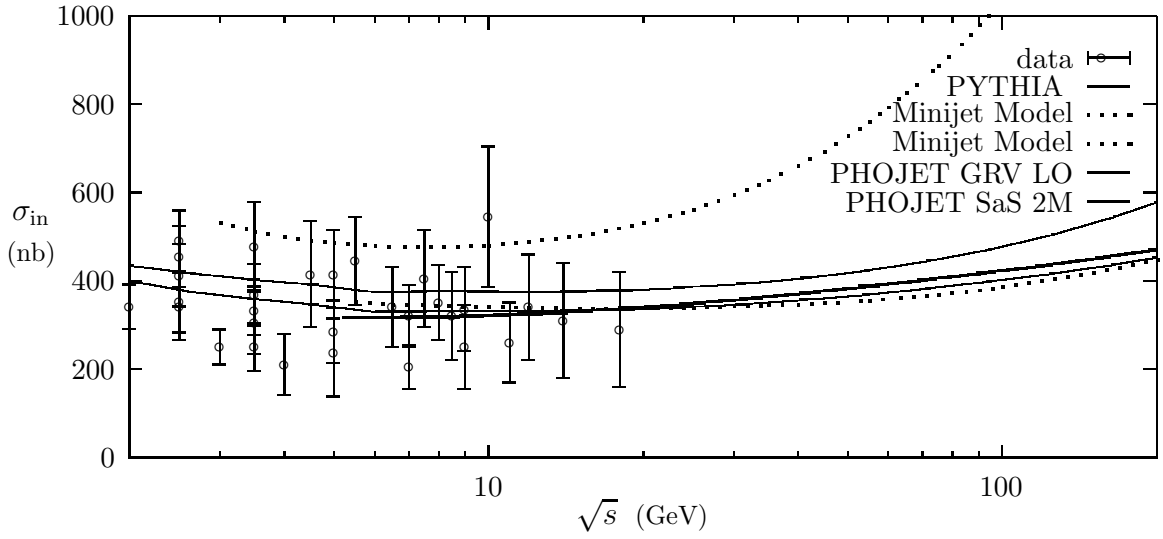

Figure 14: *Inelastic photon-photon cross sections calculated in the SaS approach [51] implemented in* PYTHIA*, the DPM model implemented in* PHOJET *[47], and an eikonalized minijet model [52] compared with data. The two curves from* PHOJET *were calculated using the GRV LO photon structure function [11] (upper curve) and the SaS 2M photon structure function [23] (lower curve). The two curves according to the unitarized minijet model are the highest and the lowest prediction presented in [52] for values of the parameters compatible with the photoproduction data.*

The eikonalized mini-jet model is well described in the literature (see e.g. [1,44]). In addition to the above-mentioned parameters such as P^{γ}_{had} and p_{Tmin} the predictions of this model depend also on $\rho(b)$, the distributions of the photonic partons in the impact-parameter space. The new feature in the calculation in [52] is that for $\rho(b)$ they use the Fourier transform of the partonic transverse momentum distribution instead of the Fourier transform of the pionic form factor which is normally the case. The former has recently been measured [53] and has the form, in agreement with the expectations of perturbative QCD, $dN_{\gamma}/dk_t^2 = 1/(k_t^2 + k_0^2)$ with $k_0 = 0.66 \pm 0.22$ GeV. Interestingly, the normal usage of pionic form factor corresponds to $k_0 = 0.735$. Predictions of the model are shown by the dotted lines in Fig. 14.

5.2 Production of hadrons and jets

In order to illustrate characteristic differences and similarities between $\gamma\gamma$, γp, and pp collisions we first show comparisons at fixed CM energy. Since elastic hadron-hadron collisions usually are excluded in studies of inclusive secondary distributions, we also exclude the analogous ones for the photon-induced reactions, i.e. the quasi-elastic diffractive channels $\gamma\gamma \to V + V'$, $\gamma p \to V + p$ ($V = \rho, \omega, \phi$) but we include all other diffractive processes.

First we show the transverse momentum distribution in Fig. 15. Both PYTHIA and PHOJET show a similar behaviour and agree very well with the behaviour of the data in Fig. 13b. In fact the distributions from both models for $\gamma\gamma$ interactions are very similar, differences between

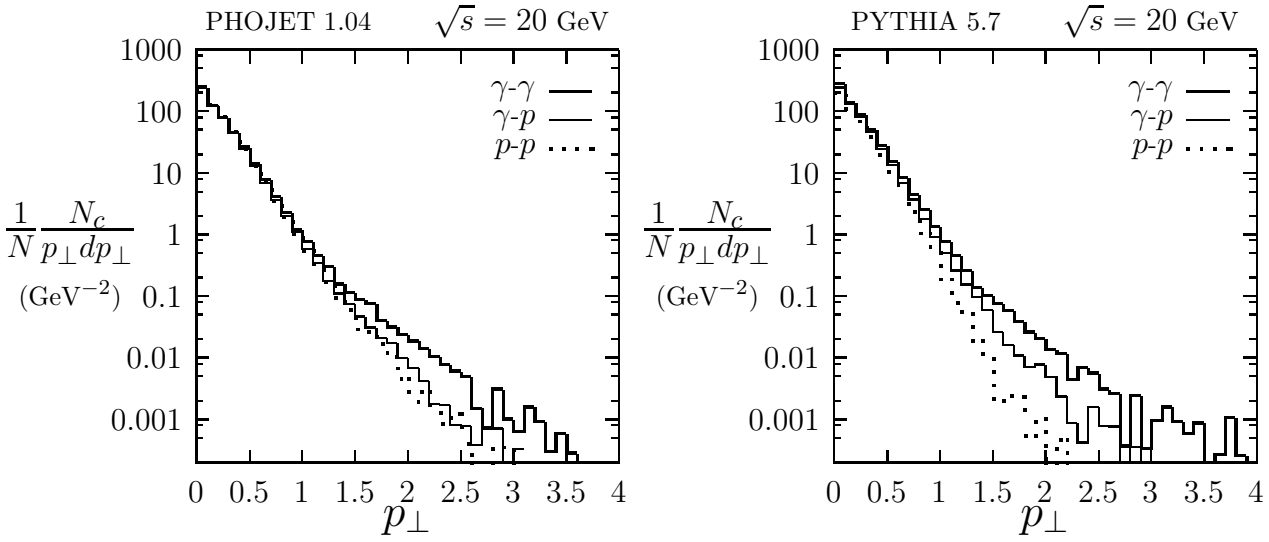

Figure 15: *Comparison at the collision energy $\sqrt{s}$ = 20 GeV of the transverse momentum distribution in invariant form for all charged hadrons produced in pp, γp and $\gamma\gamma$ collisions. The calculation was done with* PHOJET *(left) and* PYTHIA *for inelastic collisions.*

the two models appear mainly for *pp* collisions. These differences are probably due to the use of different parton distribution functions and cutoffs for minijets. As expected, at low p_T, the

$\sqrt{s}$	10	10	10	20	20	20
Quantity	*pp*	γp	$\gamma\gamma$	*pp*	γp	$\gamma\gamma$
n_{ch}	6.39	6.38	6.80	9.17	9.15	9.64
n_{π^-}	1.94	2.28	2.76	3.10	3.40	3.92
$n_{\bar{p}}$	0.06	0.10	0.14	0.122	0.17	0.22
$< p_{\perp ch} >_{centr.\eta}$ [GeV/c]	0.36	0.36	0.39	0.37	0.38	0.40

Table 1: *Comparison of average quantities characterizing hadron production in nondiffractive pp, γp and $\gamma\gamma$ collisions according to* PHOJET *at CM energies between 10 and 20 GeV.*

distributions of $\gamma\gamma$, γp, and *pp* collisions are very similar, while the fraction of hard interactions in minimum bias interactions rises from *pp* to γp to $\gamma\gamma$ collisions. The reason for this is the direct photon interaction and the fact that the photon structure function is considerably harder than the proton one. In $\gamma\gamma$ collisions it is easy to observe already with moderate statistics hadrons with transverse momenta approaching to the kinematic limit.

However, the differences in the hard scatterings hardly influence such average properties of the collision as average multiplicities or even average transverse momenta. This can be seen from Table 1, where we collect some average quantities characterizing nondiffractive *pp*, γp and $\gamma\gamma$ collisions in PHOJET at CM energies of 10 and 20 GeV. The total and charged multiplicities at all energies are rather similar to each other in all channels. The differences in the multiplicities of non-leading hadrons like π^- and $\bar{p}$ are more significant and we find them

at all energies rising from pp to γp to $\gamma\gamma$ collisions. Also the average transverse momenta rise as expected from pp to γp to $\gamma\gamma$.

Next we consider an example of hadron and jet production in e^+e^- collisions. In Fig. 16 the $e^+e^- \to e^+e^-X$ cross section is shown as a function of the visible photon-photon energy. Also shown in this Figure is the cross section for events with jets ($p_T^{jet} > 5$ GeV/c). We predict that nearly all events have jets at large W_{vis}.

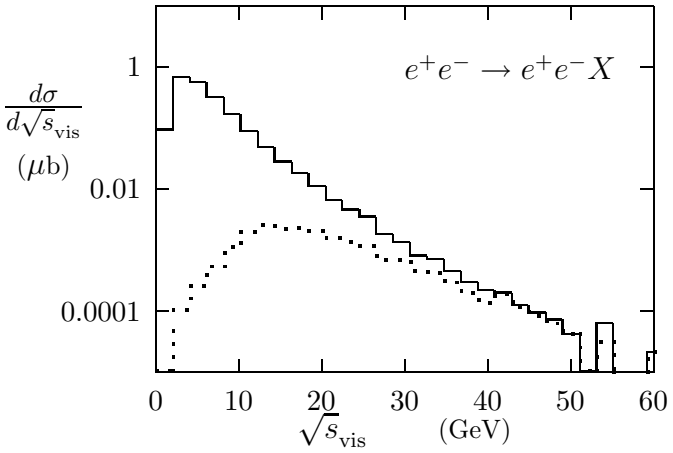

Figure 16: *Cross section at $\sqrt{s} = 175$ GeV as function of the visible $\gamma\gamma$ CM energy with cuts 1+2+3 on the final state system (full line) and for events with jets after the application of cut 1 (dotted line), (calculated with* PHOJET*; the cuts are defined in sec. 4).*

Studies at LEP1 have started recently showing that measurements of minimum bias events are indeed possible. For example, Fig. 17 shows that small p_T values are accessible. No detailed comparison between the multipurpose Monte-Carlo generators such as PHOJET and PYTHIA has yet been done with the existing LEP1 data. Instead, we show here the Aleph [56] results on the W_{vis} distribution and on the charged track p_T distribution for minimum bias untagged events compared to a specific in-house $\gamma\gamma$ event generator. The data has been modelled by a sum of four contributions (Fig. 17). The bulk of the data is described by a VMD model which includes only limited p_T with respect to the $\gamma\gamma$ direction, and has been tuned to the data. At high p_T and W_{vis} the data require additional contributions from QCD. These are separated into the direct process (labelled QPM), and the sum of single- and double-resolved processes (labelled QCD–multijets).

5.3 Measurement of the $\gamma\gamma$ hadronic cross section

In untagged two-photon events the photons are nearly on-shell. The measurement of $\sigma_{tot}^{\gamma\gamma}$ is not so much limited by statistical accuracy as by a precise description of competing processes, such as beam-gas or beam-wall scattering, annihilation reactions, and a careful simulation of the process itself. The invariant mass from beam-gas scattering is effectively limited to ≈ 15 GeV by the kinematics of electron scattering off slowly moving nucleons. It can be suppressed by requiring the event vertex to be at the interaction point. The contribution from the annihilation

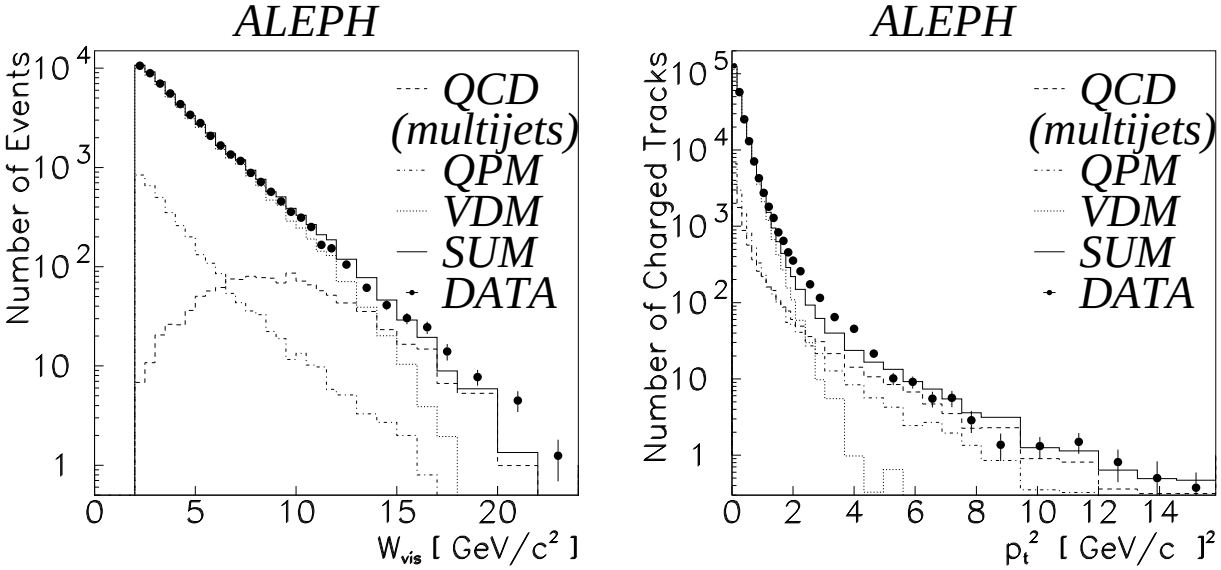

Figure 17: *(a, left) Visible energy distribution. (b, right) Transverse momentum distribution.*

process "$e^+e^- \rightarrow$ hadrons" can be reduced by requiring the average rapidity of the observed hadrons to be non-zero, while in the "$e^+e^- \rightarrow$ hadrons $+ \gamma$" process the average rapidity of the hadrons is kinematically related to the invariant mass of the hadrons. Furthermore, the different s-dependence of various processes helps their identification.
The event characteristics are dominated by the Vector Dominance process, which accounts for about 70 to 80% of the events according to present models. Much information from two-photon events disappears along the holes in the detectors around the beams. As a hardware solution to this problem is not envisaged by the LEP experiments, one has to cope with partial event information; 30 to 50% of the hadronic energy is lost in the forward region, and the fraction increases with the $\gamma\gamma$ invariant mass and LEP beam energy. Some useful information can be collected from small-angle electromagnetic detectors. At low $\gamma\gamma$ invariant mass the measurements are limited by trigger requirements. Unfolding of the true $\gamma\gamma$ mass distribution from the data with the help of event simulation is imperative, and it gives rise to model dependence in the cross section. Results are expected up to about 80 GeV, somewhat below the Z^0 mass.

Interesting studies can be performed at LEP2 with double tag $\gamma\gamma$ events using Very Small Angle Tagger (VSAT) detectors due to the high enough cross section for the polar angle region (2 - 15 mrad) covered. The DELPHI collaboration had already obtained some new results studying the single tag events in their VSAT [54] (similar detectors are currently being used in OPAL or upgraded in ALEPH and L3). The double tag mode is attractive due to the possibility of a direct measurement of both the hadronic invariant mass produced and the absolute momentum transfers squared for both photons. Taking into account the experimental constraints and the efficiency of the hadronic system registration, for 500 pb^{-1} of data, we expect about of 6000 VSAT double tagged events per experiment.
In Fig. 18 the $\gamma\gamma$ invariant mass distributions are illustrated for the visible W_{vis} (black circles), the true W_{true} (solid line) and W_{tag} (triangles) reconstructed from the tag measurements. Also

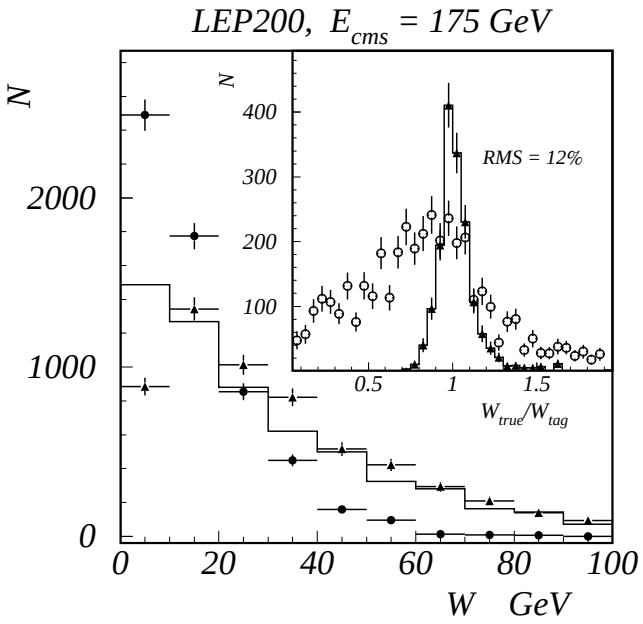

Figure 18: *Distribution in the number of events according to the various hadronic mass determinations.*

displayed is the ratio W_{true}/W_{tag} shown for two regions of W_{true}, above 40 GeV (triangles and solid line) and below (white circles). It appears that for W above 40 GeV, there is a good agreement between the W_{tag} and W_{true}. This means that one expects reliable results because there is little need to apply unfolding procedures in that region. The conclusion from this picture is that the extraction of the total $\gamma\gamma$ cross-section $\sigma_{\gamma\gamma}$ is possible in a wide region indeed: even above 80-90 GeV the statistics available is greater than 100 events.

Summarizing the above we can say that LEP2 will open a new opportunity to obtain reliable values of total $\sigma_{\gamma\gamma}$ for a $\gamma\gamma$ central energy up to 80 GeV (100 GeV) in the untagged (double-tag) case. This will increase five times the presently accessible range [55] (see Fig. 14). The extrapolation of the cross section for virtual photons in the double-tag case to $Q^2 = P^2 = 0$ should be safe since the average virtualies ($\sim 0.5\,\mathrm{GeV}^2$) are much lower than where HERA sees a strong x dependence in $F_2^p(x, Q^2)$. The uncertainty in the extrapolation will further be reduced by future HERA measurements at low Q^2. Finally, double-tag events provide a non-trivial check of hadronization models (see also sec. 3 in [4]).

5.4 Semihard quasidiffractive processes

We consider now the exclusive or semi-exclusive production of neutral mesons M

$$\gamma\gamma \to M\ M', \qquad\qquad \gamma\gamma \to M + X \tag{22}$$

in the semihard region

$$W^2 \gg p_\perp^2 = |t| \gg \mu^2, \;\; W^2 = (p_{1\gamma} + p_{2\gamma})^2, \;\; t = (p_{1\gamma} - p_M)^2, \;\; \mu = 0.3\,\mathrm{GeV}. \tag{23}$$

Here M is a vector ($V = \rho^0, \omega, \phi, ...\Psi$), or pseudoscalar ($P = \pi^0, \eta, \eta'$), or tensor ($T = a_2, f_2, f'$) neutral meson and X is a hadron system with not too large invariant mass $M_X^2 \lesssim |t|$. Such processes are discussed in a number of papers (see, for example, [57–59]).

The condition $|t| \ll W^2$ determines these processes as quasi-Regge ones. In the production of the vector meson V vacuum quantum numbers are transferred from the photon to the meson. The energy dependence of these processes is determined by the Pomeron singularity. In the production of pseudoscalar P or tensor T mesons the corresponding singularity is the odderon. In perturbative QCD (pQCD), the Pomeron (PP) and the odderon (PO) have the same status, however, the current data do not indicate unambiguously the odderon contribution to the total cross sections.

In the lowest order of pQCD the processes (22) are described by diagrams with two quark exchange. Their contribution to the cross section $d\sigma/dt$ decreases as W^{-4} with increasing W [57]. However, the contribution of the diagrams with the gluon exchange does not decrease with W while t is fixed. For the production of vector mesons V the lowest nontrivial diagrams of pQCD corresponds to the two-gluon exchange and for the production of P and T mesons to the three-gluon exchange. The current lowest order calculations are performed in this approximation [57, 58]. In Tab. 2 the expected event rates are given.

It should be emphasized that the lowest order calculations (LO) provide a lower limit of the expected event rates, as, at high enough energies, higher-order terms in the perturbative series such as $\alpha_s(p_\perp^2) \ln(W^2/p_\perp^2)$ become large and lead to a considerable increase of the cross sections. For the PP case, this effect has been calculated in the leading logarithm approximation (LLA) (see Refs. [60] and references therein). Defining $z = 3\alpha_s/(2\pi) \ln W^2/W_0^2$ the expression for the differential cross section can be written [59], as a power series in z, *i.e.*

$$\frac{d\sigma}{dt} = \frac{d\sigma_{\rm 2gluon}}{dt}(1 + \sum_{n=1}^{\infty} c_n z^n) = \frac{d\sigma_{\rm 2gluon}}{dt} \, |K(W^2, t)|^2. \tag{24}$$

The value of z is very sensitive to the choice of parameters: for example, taking $\alpha_s = .2$ (small), $W_0^2 = 4(p_T^2 + m_V^2) = 16$ GeV^2 (large) and $W_{min} = 15$ GeV one obtains the conservative estimate $z = .25$. LEP2 can get statistics in the region $z = .25 - .5$. If $z \geq .5$, the perturbative series needs to be summed to all orders and the striking power behaviour of the cross sections emerges, *i.e.*

$$\frac{d\sigma}{dt} \sim f(W, t) \left(\frac{W^2}{W_0^2}\right)^{2\omega_0}, \tag{25}$$

where $1+\omega_0$ is the "intercept" of the BFKL Pomeron and the W dependence in $f(W, t)$ is weak. A corresponding strong enhancement over the two-gluon exchange results is thus anticipated. For large values of z we have the LLA result $2\omega_0 = (12/\pi)\alpha_s(t) \ln 4$ leading eventually to a violation of the Froissart bound. At large enough W^2 this growth should be stopped by unitarity to satisfy approximately $K(W^2, t) < 25$ [57]. The PO estimations in [60] show that there is an increasing function of a parameter like z also for the PO.

In the case of J/Ψ production there exists a prediction [59] which takes into account the coupling of the reggeised gluons to the $c\bar{c}$-J/Ψ system. For $p_T^2 = -t \ll M_\psi^2$ and large z the

cross section is given by

$$\frac{d\sigma(J/\Psi J/\Psi)}{dp_T^2} = 16\pi^2\alpha^2(\alpha_s C_F)^4 \frac{\pi^3}{4} \frac{\exp(16z\ln 2)}{(7\pi\zeta(3)z)^3} \left(\frac{c_\psi f_\psi}{M_\psi^2}\right)^4 \ln^4 \frac{M_\psi^2}{p_T^2}, \tag{26}$$

where $c_\psi = 3/4$ and $f_\psi = 0.38$ GeV.

process	$W_{\min}$ (GeV	$\lvert t\rvert_{\min}$ (GeV^2)	$\Theta_{\min}$ (mrad)	LO	LLA Eq. (25)	LLA Eq. (26)
$\rho\rho$	15	9	-	0.8	180/140	
	15	4	87	9.2		
	15	4	175	2.4		
ρX	15	9	-	100	23000/18000	
	25	16	-	13	2300/2100	
	15	4	87	840		
	15	9	87	240		
$J/\Psi J/\Psi$	15	-	-	10	2500/2000	
	15	4	87	1.4		570
	15	4	175	0.5		320
	25	4	87	0.5		440
	25	4	175	0.1		220
$J/\Psi X$	15	-	-	120	26000/21000	
$\pi^0 X$	10	5	-	180		

Table 2: *Number of expected events for LEP II with an integrated e^+e^- luminosity of 500 pb^{-1}. The calculation was done for anti-tagged e^+e^- events with $\Theta_e \leq 30$ mrad.*

In Tab. 2 we present the number of expected events for LEP2 based on the two regimes (LO and LLA) described above. Since one does not know at which energy the asymptotic predictions become valid we expect the number of experimentally observed events to be bracketed by the two sets of predictions. Further uncertainties are associated to the choice of α_s and W_0 and the fact that the enhanced rates are obtained using the large z approximation in solving the BFKL equation. More modest enhancements can be expected for the z values typical of LEP2 (see the numerical studies in [59]) . The values for the $\gamma\gamma$ cross sections in lowest order are the following: for the J/Ψ production we use the total cross sections obtained in [58], for ρ^0 and π^0 the cross section corresponds to the region $-t \geq |t_{min}|$. In the calculations, the photon-photon energy was restricted to $W_{\gamma\gamma} \geq W_{min}$. Furthermore, results are given for the cross sections demanding the meson to emerge at angles larger than Θ_{min}. For the estimation of the effects of BFKL Pomeron we use the K factor calculated for the process $\gamma\gamma \to \gamma\gamma$ via two $c\bar{c}$ pairs [60]. To show the strong dependence of the results on the limitation of K, two sets of numbers are given (last row), for $K \leq 25$ and for $K \leq 20$. In addition, the event rates according to Eq. (26) (neglecting unitarity corrections) are given. Note that the numbers obtained with the constraint on Θ_{min} are calculated with a fixed value of $\alpha_s = 0.32$ whereas for the other numbers running α_s was used.

In conclusion, it appears that the study of diffractive phenomena in the semi-hard domain may yield interesting information on the nature of the Pomeron.

6 Large-p_T processes and NLO phenomenology [10]

As it is the case in the study of the proton structure the production of jets or hadrons at large p_T in $\gamma\gamma$ collisions is complementary to the deep-inelastic scattering of a real photon: indeed the latter reaction essentially probes the quark distribution while large p_T phenomena are also sensitive to the gluon distribution. In order to reliably understand the hadronic structure of the photon both types of processes (as well as heavy flavor production, see next section) should be studied and compared to the theory. Taken together, they will allow the determination of the parton distributions in the photon. For this purpose, we discuss below the jet inclusive cross section at the next-to-leading order (NLO) in QCD and related processes in the case of anti-tag or single tag experiments. The possibility to identify the gluon jet in three-jet events is also considered.

6.1 The structure of the hard process

Large p_T processes involving real photons are rather complex. This arises from the fact that the photon couples to the hard sub-process either directly or through its quark or gluon contents. The cross section for the production of a jet of a given p_T and pseudorapidity η can therefore be decomposed as (D: direct, SF: structure function, DF: double structure functions)

$$\frac{d\sigma}{d\vec{p}_T d\eta} = \frac{d\sigma^D}{d\vec{p}_T d\eta} + \frac{d\sigma^{SF}}{d\vec{p}_T d\eta} + \frac{d\sigma^{DF}}{d\vec{p}_T d\eta} \tag{27}$$

where each term is now being specified. In the NLO approximation [35] the "direct" cross section takes the form

$$\frac{d\sigma^D}{d\vec{p}_T d\eta}(R) = \frac{d\sigma^{\gamma\gamma\to jet}}{d\vec{p}_T d\eta} + \frac{\alpha_s(\mu)}{2\pi} K^D(R;M). \tag{28}$$

with the corresponding diagrammatic decomposition shown in Fig. 19a and b. The parameter R specifies the jet cone size, while μ and M are the renormalization and factorization scales respectively. When one photon couples directly and the other one through its structure function, it leads to

$$\frac{d\sigma^{SF}}{d\vec{p}_T d\eta}(R) = \sum_{i=q,G} \int dx_1 F_{i/\gamma}(x_1, M) \frac{\alpha_s(\mu)}{2\pi} \left(\frac{d\sigma^{i\gamma\to jet}}{d\vec{p}_T d\eta} + \frac{\alpha_s(\mu)}{2\pi} K^{SF}_{i\gamma}(R;M,\mu) \right) + 1 \to 2 \tag{29}$$

where some diagrams representative of the $\mathcal{O}(\alpha_s)$ and $\mathcal{O}(\alpha_s^2)$ terms on the right hand side are shown in Fig. 19c and d, respectively. The underlined diagrams in Fig. 19b and c are in fact the same but they contribute to different regions of phase space. When the final state quark is not collinear to the initial photon (as in Fig. 19b)) the exchanged propagator has a large virtuality (shown by the fat line) and the corresponding contribution is associated to the hard subprocess K^D. When the final quark is almost collinear to the initial photon (as

[10] P. Aurenche, M. Dubinin, R. Engel, J.P. Guillet, J. Ranft, Y. Shimizu, M.H. Seymour

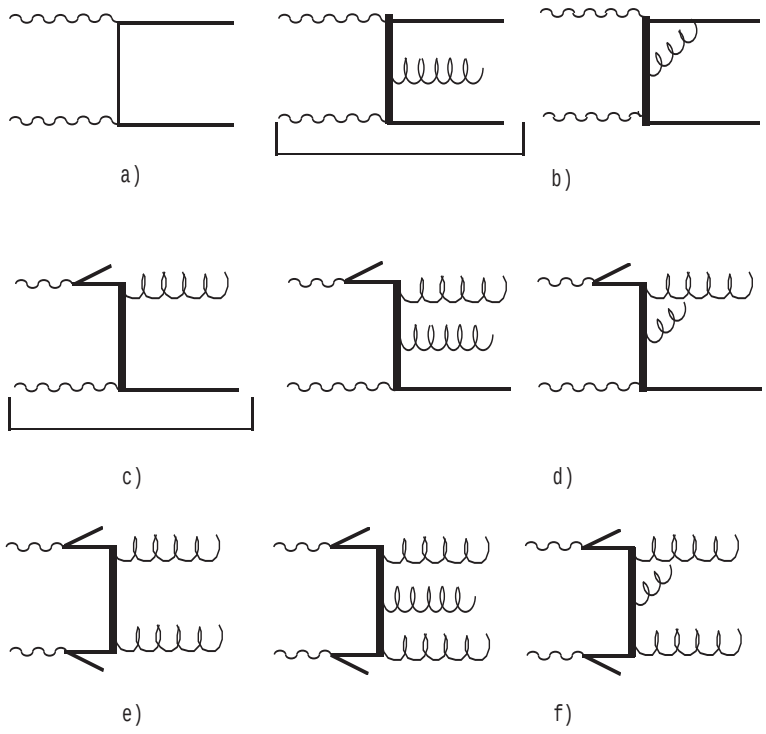

Figure 19: *Some diagrams contributing to jet production in $\gamma\gamma$ collisions in the NLO approximation.*

in Fig. 19c)) the virtuality of the exchanged propagator is small and the interaction is soft (long range). Roughly speaking the factorization scale M separates the hard region from the soft region and changing this arbitrary scale shifts contributions from $d\sigma^D$ to $d\sigma^{SF}$ but clearly should not affect the sum $d\sigma^D + d\sigma^{SF}$ [61]. A similar compensation occurs between $d\sigma^{SF}$ and $d\sigma^{DF}$ (see Fig. 19d and e). In conclusion, only the sum eq. (27) has a physical meaning and it is not legitimate to associate $d\sigma^{SF}$ and $d\sigma^{DF}$ to experimentally measured "once resolved" and "twice resolved" components. To illustrate quantitatively the variation of the theoretical predictions under changes of M and μ we consider the production of jets at $p_T = 10$ GeV/c and $\eta = 0$: Fig. 20a is obtained when setting arbitrarily $K^D = K^{SF} = K^{DF} = 0$ (the so-called leading order (LO) predictions) while Fig. 20b takes into account the full expressions: the gain in stability is remarkable despite the fact that no saddle-point or extremum is found [35]. In the following we always use for definiteness $M = \mu = p_T$.

6.2 Transverse momentum and rapidity distributions

In order to compare theory and experiment one must convolute the above cross sections with the Weizsäcker-Williams spectrum of quasi-real photons emitted by the electrons, taking into account the experimental conditions. The usual antitagging conditions defined in sec. 4 are used here ($\theta_e < 30$ mrad or $E_e < 1\ GeV$). The appropriate Weizsäcker-Williams spectrum is given in eq. (14). We display in Fig. 21 the jet p_T distribution, the jet pseudo-rapidity being integrated in the interval $|\eta| < 1$. The complete NLO expressions are used. The solid curve is the prediction when using the full AFG parton distributions (with a VMD input at

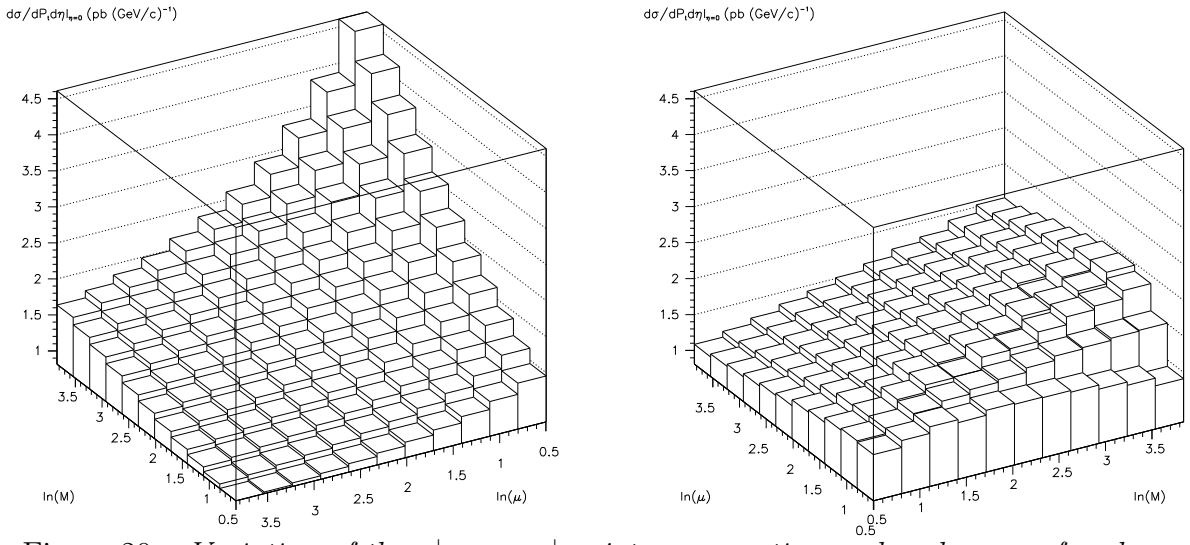

Figure 20: *Variation of the $e^+e^- \to e^+e^-$ jet cross section under changes of scales: a) leading logarithmic approximation; b) next-to-leading logarithmic approximation.*

$Q_0^2 = .5$ GeV^2) [19], while the dashed curve is obtained when one artificially sets the VMD component equal to 0. More precisely, in the latter case, the quark and gluon densities are vanishing at Q_0^2 and they are generated by the evolution equations at larger Q^2. It is clearly seen that the VMD component is quite important at $p_T = 5$ GeV/c (about 40%) but rapidly decreases as p_T increases since it is less than 10% at $p_T = 20$ GeV/c. One may note that the VMD component of the quark is also tested in photon structure function studies but large p_T processes are also very sensitive to the VMD component of the gluon which dominates for $x < .5$. With the luminosity expected at LEP2 the error bars in the data will be sufficiently small to constrain the size of the VMD input.

As mentioned in the structure function section above it will be possible to probe the virtual photon structure in deep-inelastic type experiments. We show here that it can also be probed in jet studies. Using the tagging conditions $.2 < Q^2$ (GeV^2) $< .8$ and $z_\gamma < .5$, typical of LEP2, on one photon and the usual anti-tagging condition on the other, one still obtains an appreciable jet cross section as shown on Fig. 21: about 100 events with $p_T = 10 \pm 1$GeV/c are expected. Let us remark that, thanks to the usual VMD form-factor, the VMD contribution is rapidly reduced when considering tagged electron (it is reduced by roughly 75% when going from a real photon to a photon of virtuality $Q^2 = .5$ GeV^2).

Despite the warnings given above, we display in Fig. 22 the break-up of the single inclusive jet cross section, integrated in the range $|\eta| < 1$, into the DIR, SF and DF components. These curves can serve useful purposes when comparing these analytic calculations with those based on Monte-Carlo generators. Of course, the size of the various components depend strongly on the choice of the factorization scale (here we use $M = \mu = p_T$). In the figure, obtained using the leading logarithmic expressions for the sub-processes we see that DF component dominates the lower end of the distribution but is less than 20% at $p_T = 20$ GeV/c. Nowhere does the SF terms dominate. In Fig. 23 we show the rapidity dependence for $p_T = 5$ GeV/c and $p_T = 15$ GeV/c of the various components both in the LO and the NLO approximation. One sees that the pattern of higher corrections is quite different for the different subprocesses:

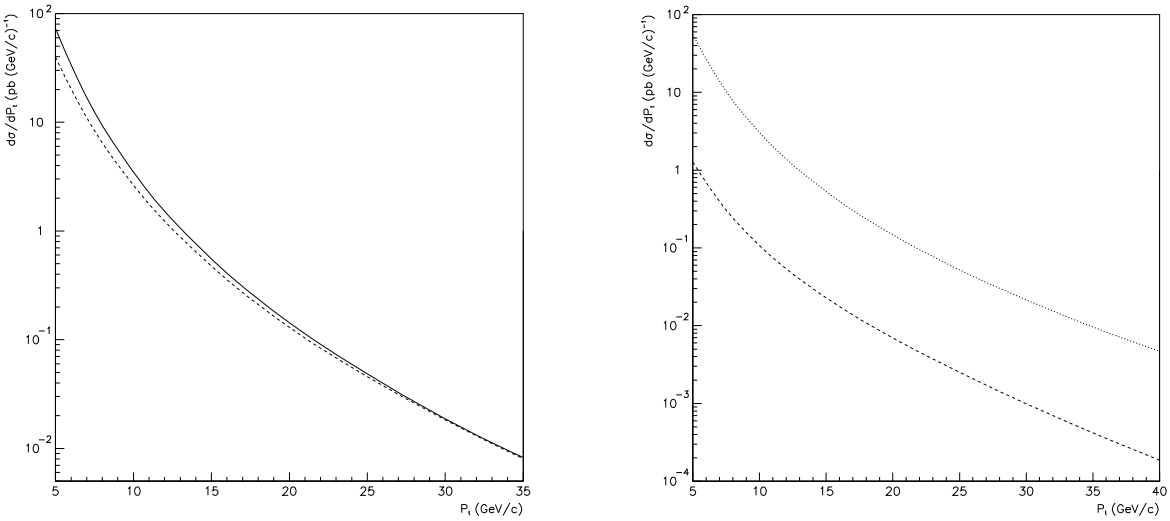

Figure 21: *Jet pt distributions. Left: The NLO cross section using the full structure functions (solid line) compared to the case when only the perturbative part is kept (dashed line). Right: the same as above (solid line) in the LO approximation and the cross section when one of the photon is tagged (dashed line).*

the DF component is appreciably increased by the higher-order corrections (about 40%) while the DIR component is decreased and (roughly 15%) the SF component remains stable. This pattern of higher order corrections is independent of the transverse momentum or rapidity. It is interesting to remark that at $p_T = 15$ GeV/c the hierarchy of cross sections is reversed when including the higher order corrections with the DF term dominating over the DIR one despite the fact that the overall cross section is not affected very much. In conclusion, one may say that the higher-order corrections affect the structure of the cross section more than its overall size.

It will be very useful to study a more exclusive observable namely the di-jet cross section. Quite interesting phenomenology is coming out of HERA [62]: it allows to separate on an experimental basis events dominated by the direct component from those dominated by the photon structure function. For an application of this technique to $\gamma\gamma$ reactions we refer to the "High-p_T" section of [4]. NLO calculations are in progress [63].

Recently data on jet distributions have been published by the TOPAZ [64] and AMY [65] collaborations. The above calculations are in good agreement [35] with the single jet distribution of TOPAZ when using the AFG parton distributions [19] while both the NLO predictions [63] and the PHOJET [66] results using the GRV parametrizations [11] fall below the data. In contrast, a rather good agreement, at least at large p_T values, is found with the two-jet data of TOPAZ in [63] and [66].

A word of caution should be said concerning large p_T phenomenology. Even at LEP2 we are dealing with rather low p_T jets and the comparison between the theoretical predictions, at the partonic level, and the experimental distributions at the hadronic level may not be easy because of the non negligible contribution to the jet transverse momentum from the "underlying event" [67]. Good event generators are required to understand this point and also a lot should

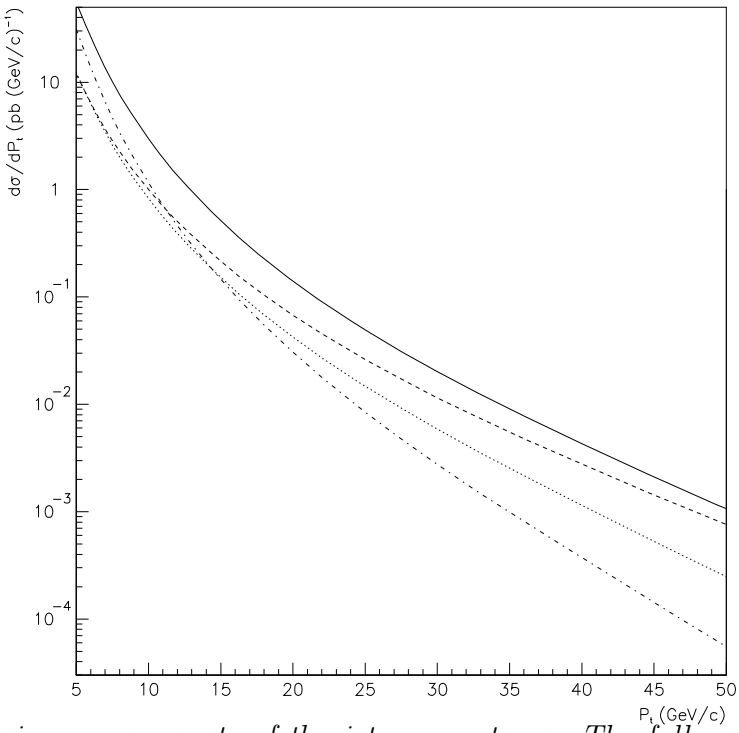

Figure 22: *The various components of the jet p_T spectrum. The full cross section: full line; the DIR component: dashed; the SF component: dotted; the DF component: dash-dotted.*

be learnt from present HERA studies. To avoid this difficulty it will be extremely interesting to consider the single hadron inclusive distribution which probes the same dynamics as jet production. New parameters come into play through the fragmentation functions of partons into hadrons but these distributions should soon be rather well constrained as several groups are at present extracting NLO parametrizations of fragmentation functions using data from both e^+e^- colliders and pp colliders [68]. Concerning lower energy data, the situation concerning single hadron production is rather confusing and paradoxical as the experimental results [69] are much above the NLO theoretical predictions [70] at large p_T (where the DIR term is predicted to dominate) while they agree with the theory at lower p_T. Data are eargerly awaited to clarify this point.

6.3 Three-jet events and the separation of gluon jets

The first direct evidence for gluon jets was seen by the PETRA experiments as three-jet events, $e^+e^- \to q\bar{q}g$, where all three partons have high energy and are well-separated in angle. Ever since, one of the important aims of QCD studies has been to measure the similarities and differences between quark and gluons jets, as well as collective quark-gluon phenomena such as the string effect [71]. One of the important questions is to what extent such effects can be described by perturbative QCD, rather than non-perturbative models. However, many of the studies are inconclusive on this issue, because at any given energy, most non-perturbative models can be tuned to mimic the perturbative effects, and it is only in the energy-dependence that definitive differences can be seen. But comparing experiments at different energies typically

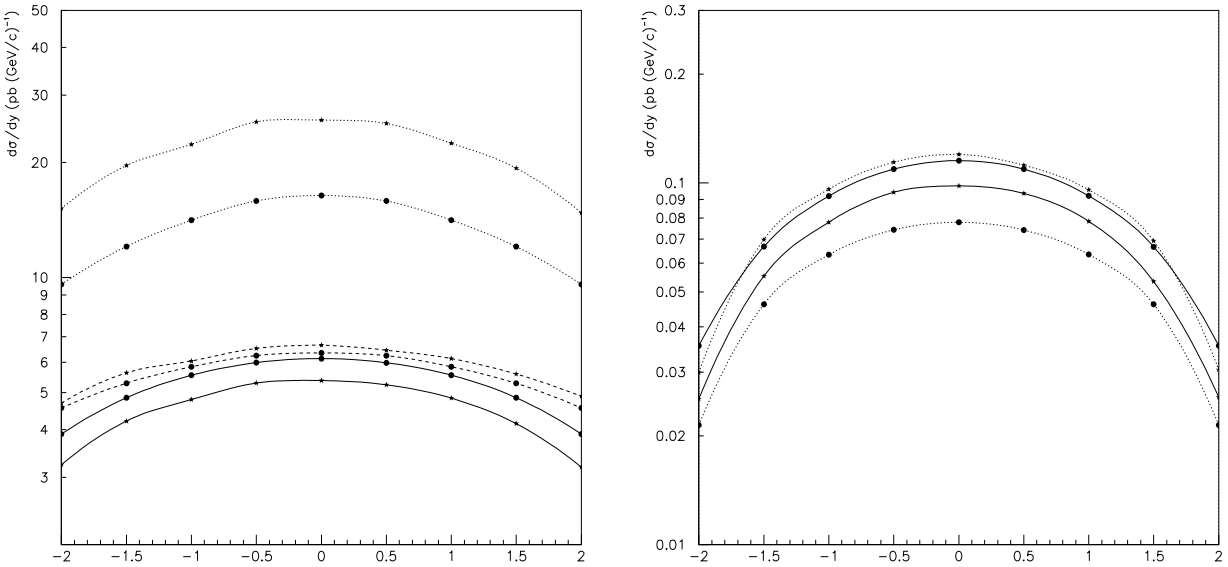

Figure 23: *The jet rapidity distributions at fixed p_T. The meaning of the curve is as in the previous figure. The dotted lines are the LO results while the starred line are the NLO results. Left: $p_T = 5$ GeV/c; right: $p_T = 15$ GeV/c.*

involves large uncorrelated systematic errors. In $\gamma\gamma$ collisions on the other hand, one can study a wide range of energies in the same experiment, and can thus study energy-dependent effects much more reliably.

We can make a rough estimate of the three-jet rate by taking the leading logarithmic approximation to the total two-jet rate [72] and simply multiplying it by a factor of α_s as an estimate of the fraction of three-jet events. We require each jet to have a transverse momentum above $p_{t_{\min}}$ both with respect to the beam axis and each other, and hence obtain

$$\sigma(s, p_{t_{\min}}) = \frac{4}{3}\left(\sum_q e_q^4\right)\frac{N_c\alpha^4}{\pi p_{t_{\min}}^2}\log\frac{s}{p_{t_{\min}}^2}\log^2\frac{s}{m_e^2}\times\alpha_s.$$

It is worth noting that the smallness of α_s cannot be compensated by any large logarithms, because the appropriate logarithms are $\log W^2/p_{t_{\min}}^2$ and the W^2 distribution is dominated by $W^2 \sim p_{t_{\min}}^2$. Nevertheless, we obtain around 10^4, 10^3 and 10^2 events in 500 pb^{-1} for $p_{t_{\min}} = 5,\ 15$ and 35 GeV respectively. For such studies it is important to know which jet is the gluon. The cleanest way to do this is by flavour tagging the quark jets, but this severly reduces the rate. In e^+e^- annihilation, the fact that the gluon's energy spectrum is softer than the quark's was used, by always calling the softest of the three jets the gluon. By explicit analytical integration of the full five-dimensional matrix element for $\gamma\gamma \to q\bar{q}g$ down to a distribution over the energies of the quarks [73], we find that the same is also true for $\gamma\gamma$ collisions (Fig. 24, see [73] for further details). Thus the gluon jet in three-jet events can be statistically tagged by calling it the softest jet.

Although a more complete study incorporating realistic detector cuts and the effects of hadronization is clearly needed, it seems hopeful that a sample of three-jet events could be isolated and a study of the energy-dependence of quark-gluon jet effects made at LEP2.

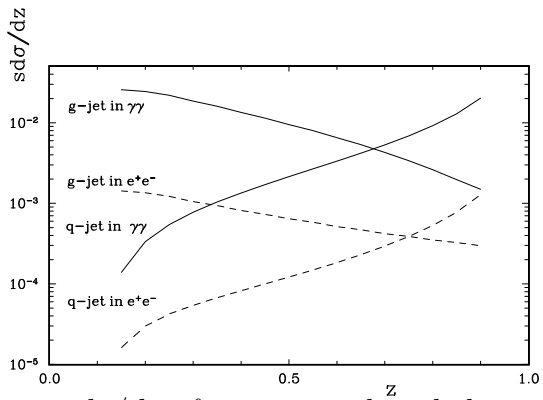

Figure 24: *Differential spectra $sd\sigma/dz$ of parent quark and gluon in the reactions $e^+e^- \to q\bar{q}g$ and $\gamma\gamma \to q\bar{q}g$*

6.4 Role of the experimental cuts on the inclusive jet spectrum

We have seen in sec. 4 that the radiative production of Z^0 bosons provides an important background to $\gamma\gamma$ physics when one looks for rare events such as large p_T jets. Various cuts

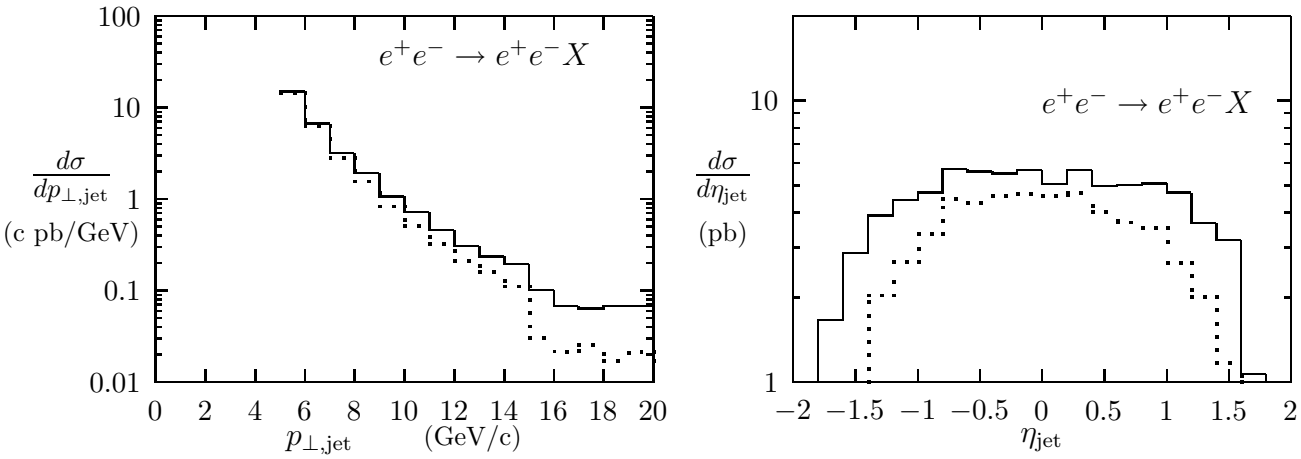

Figure 25: *Jet cross section for events satisfying cut 1 (full line) and cut 1+2+3+4 (dotted line). Left: distribution in p_T with $|\eta_{jet}| < 1$; right: distribution in η_{jet} for fixed $p_T = 7$ GeV/c. (Calculated with* PHOJET*).*

have been devised which considerably reduce the background. The study of the effect of these cuts on the signal requires the use of a Monte-Carlo generator and we use here the PHOJET program [47,48]. We have checked that the unbiased jet p_T spectrum is in good agreement with the analytical results described above. In Fig. 25 we see that, as expected, only the upper end of the spectrum is reduced by the cuts (see sec. 4 for the meanings of the cuts) while at fixed p_T mainly the large $|\eta_{jet}|$ regions are reduced. The net result is that, after cuts, the rate for producing jets with $p_T \simeq 20$ GeV is comparable in the signal and in background. Needless to say that jets produced in single tag events are not affected by the background.

7 Heavy-quark physics [11]

A favourable aspect of heavy flavour production in $\gamma\gamma$ collisions compared to other $\gamma\gamma$ processes is that the heavy quark mass ensures that the separation into a direct and resolved processes is, to next-to-leading order (NLO) in QCD, unambiguous, i.e. does not depend on an arbitrary separation scale. Experimentally one may perform this separation by using single tag events (see below), by using non-diffractively produced J/ψ's, or by using the photon remnant jet, present in resolved processes, as a separator. Therefore heavy flavour production at LEP2 provides a good opportunity for simultaneously testing QCD (direct process) and measuring the poorly known gluon content of the photon (resolved processes).

7.1 Theory

We first discuss the theoretical aspects of the reaction $\gamma\gamma \to Q\bar{Q}$ where Q ($\bar{Q}$) is a heavy (anti)-quark (charm or bottom). In practice the cross section for bottom production is too small to be observed at LEP2 so, in what follows, only charm production will be considered. Figure 26 shows some of the diagrams contributing to heavy quark production in two-photon physics. Diagrams (a)-(c) are examples of the so-called direct process in which the photon couples directly to a quark. Diagram (a) is the Born term direct process which is equivalent to the Quark Parton Model (QPM), (b) and (c) represent virtual and real QCD corrections to the Born amplitude. At low beam energy the direct process is completely dominant, however at LEP2 the production of open charm in the collision of two effectively on-shell equivalent photons receives contributions in about equal amounts from the direct- and once-resolved channels diagrams (d)-(f). In Ref. [74] this process was calculated to NLO in QCD, and all theoretical uncertainties (due to scale choice, mass of the charm, and choice of photonic parton densities) were thoroughly investigated. The largest part of the resolved process is given by the photon-gluon fusion process; this property offers the possibility of measuring the gluon content of the photon which is currently poorly known. Doubly resolved processes have been calculated to give a negligible contribution for presently available beam energies [74]. In Fig. 28 the total cross section and its theoretical uncertainty is shown as a function of the center of mass energy, together with some recent measurements. LEP2 offers the possibility of a serious comparison between a fairly well understood theory and experiment with considerably more statistics than hitherto. Given this larger statistics it will be interesting to make this comparison not just for the total cross section, but also for various differential distributions. Single particle distributions in the transverse momentum and rapidity of the heavy quark are given in [74]. Correlations between the heavy quarks in the direct process, including NLO effects, have recently been studied in [75], but will be difficult to observe at LEP2.

Furthermore, the NLO prediction for the one particle inclusive transverse momentum distribution contains potentially large terms $\sim \alpha_s \ln(p_t/m)$ which might spoil the convergence of the perturbation series at $p_t \gg m$. In Ref. [76] the NLO cross section for large p_t production of heavy quarks in direct and resolved channels has been calculated in the framework [77] of

[11] M. Cacciari, A. Finch, M. Krämer, E. Laenen, S. Riemersma, G.A. Schuler, S. Söldner-Rembold

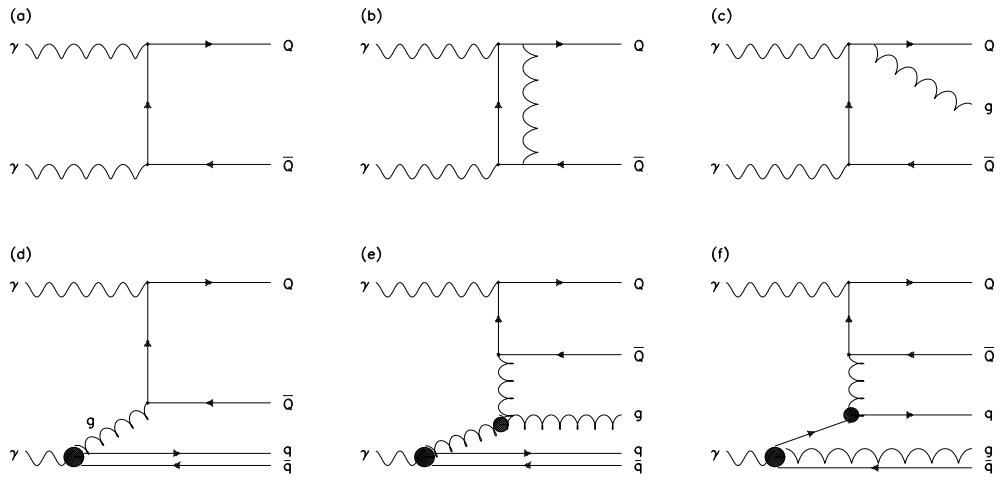

Figure 26: *Examples of diagrams contributing to heavy quark production in $\gamma\gamma$ collisions. (a) Direct contribution: Born term (QPM); (b) virtual correction to direct term; (c) real correction to direct process; (d-f) "resolved" contributions.*

perturbative fragmentation functions. This approach allows for a resummation of the large logarithmic terms and thereby reduces the scale dependence of the NLO prediction.

The process $\gamma^*\gamma \to c\bar{c}$ is considerably more suppressed than the previous one due to the photon being off-shell. The structure functions $F_2^\gamma(x, Q^2)$ (and $F_L^\gamma(x, Q^2)$) for open charm production in deep-inelastic single-tag events were calculated to NLO in QCD in [17]. It was found that the contributions from the direct (or "pointlike") and resolved (or "hadronic") separate in the variable x: above $x \simeq 0.01$ $F_2^\gamma(x, Q^2)$ is almost exclusively due to pointlike photons, and hence calculable, below this value it is mainly due to resolved photons, and essentially proportional to the gluon density in the photon, see Fig. 27a. Experimental studies of the reaction $e^+e^- \to e^+e^- D^{*\pm} X$ with one outgoing lepton tagged ("single-tag") have been done by JADE [78] and by TPC/Two-Gamma [79] at low average value $\langle Q^2 \rangle$ of the momentum transfer squared of the tagged lepton (below 1 $(\mathrm{GeV}/c)^2$) and by TOPAZ [80] at somewhat larger $\langle Q^2 \rangle$. The total number of events obtained was however very small (about 30 for TOPAZ).

Theoretical uncertainties in these quantities were investigated and are well under control. Numbers of events expected per bin in x, Q^2 over the lifetime of LEP2 are also given in Fig. 27b and in [81]. One may conclude from these that with a not too pessimistic charm acceptance (1-2%) a measurement of $F_2^\gamma(x, Q^2)$ should be feasible. Some single particle differential distributions in the transverse momentum and rapidity of the heavy quark have been studied in [81].

Let us finally mention *onia* production. The radiative decay width of the charmonium states η_c, χ_{c0} and χ_{c2} can directly be measured in two-photon collisions at LEP2. These $\gamma\gamma$ partial widths provide an important test of the non-relativistic quarkonium model. We refer to the section on resonances and exclusive states for more details. We comment here only further on the case of J/ψ.

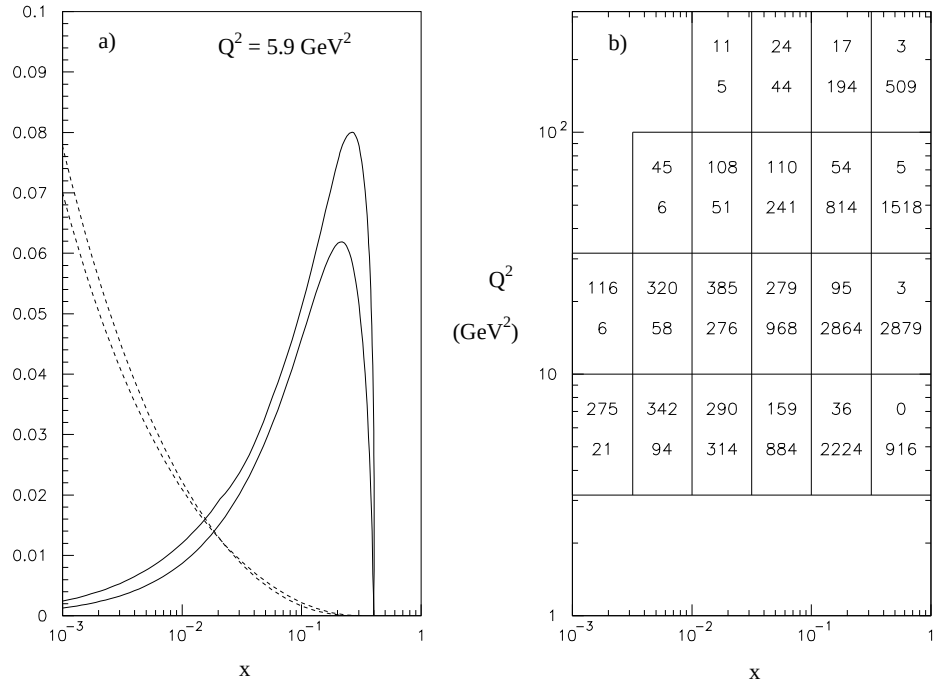

Figure 27: *a) $F_2^\gamma(x,Q^2)/\alpha$ as a function of x at $Q^2 = 5.9(\mathrm{GeV/c})^2$ for charm production at LO and NLO in QCD. The dashed line is the resolved (or hadronic) contribution (lower curve at small x: NLO, upper: LO), the solid the direct (or pointlike) (upper curve: NLO, lower: LO); b) Number of events in x, Q^2 bins. Upper number: resolved contribution, lower number: direct.*

Two-photon production of J/ψ bound states is an attractive tool to determine the gluon distribution in the photon. In contrast to the case of open heavy flavour production, J/ψ mesons are generated only via resolved photons and can be tagged in the leptonic decay modes. Higher order QCD corrections to J/ψ production in photon-gluon fusion have been calculated in [82]. Including NLO corrections, the cross section for inelastic J/ψ production in $\gamma\gamma$ collisions at LEP2 is predicted to be about 5 pb, suggesting that a measurement of this reaction may be feasible.

7.2 Experiment

We review in this section the experimental status of charm production in $\gamma\gamma$ collisions, list and evaluate presently available charm identification methods, and extrapolate published results to total charm cross sections for the purpose of comparison. We think this is useful as no such review is presently available in the literature.

Experimental measurements of charm production in $\gamma\gamma$ physics require some form of tag

to identify the presence of the charm quark. There are a number of different techniques that have been used for this in the past. They cover a spectrum in which generally the higher the selection efficiency of the tag, the larger the problems due to backgrounds from non charm contributions. These different techniques are described in the following and are summarised in Table 5 and Fig. 28. In order to enable the different experimental results to be compared we have attempted in this report to extrapolate the published results to a total charm cross section. Some caution is in order however when comparing theory and the results of different experiments in this way. This arises from the strong dependence of the cross section at low p_t on the choice of charm mass and renormalization scale. As all experimental results are made above some explicit or implicit p_t cut, extrapolating back to a total cross section increases the error on the measurement. This problem has been treated in different ways by each experiment, e.g. TOPAZ [80,83] chose only to quote a cross section in a limited acceptance. Table 3 summarizes the approach of each experiment.

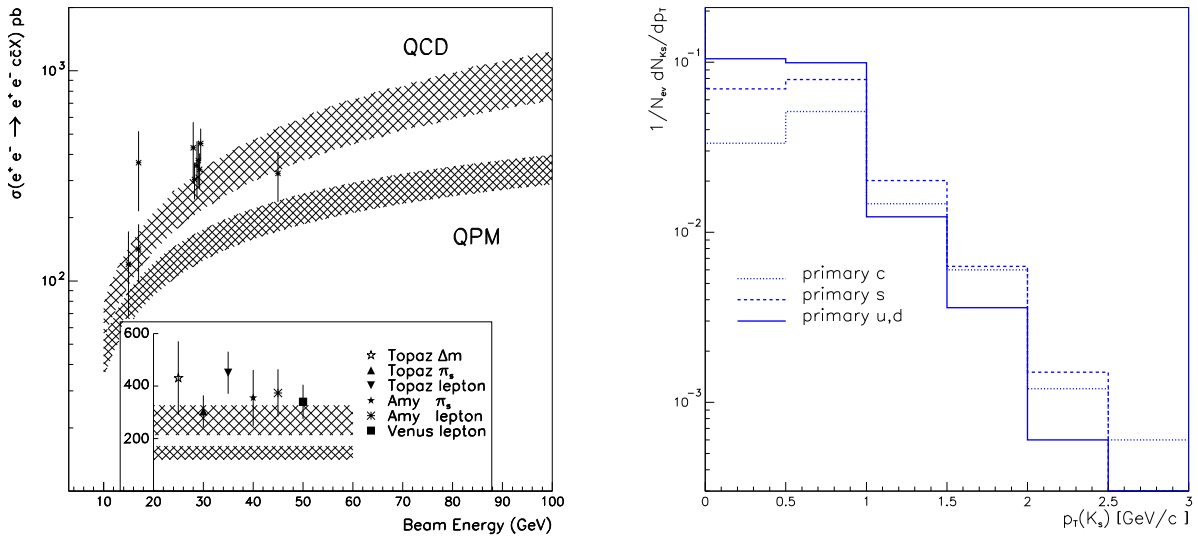

Figure 28: *Comparison of theoretical predictions and experimental results for the total charm cross section. The experimental results have been extrapolated to a total cross section from published measurements. Insert shows the results from Tristan experiments at a beam energy of 29 GeV. Results are tabulated in Table 6. The bands represent a range of theoretical predictions. See table 4 for details.*

Figure 29: *Distribution of transverse momentum $p_t(K_s)$ of K_s simulated with* PYTHIA *5.7 at $E_{\rm CM} = 91$ GeV.*

We now discuss the various charm tagging techniques in more detail. The *D^* tagging* technique exploits the fact that the available kinetic energy in the decay $D^{*+} \to D^0\pi^+$ is only 6 MeV. The signal is typically displayed by plotting $\Delta M = M_{D^{*+}} - M_{D^0}$ for all reconstructed decay product candidates. A D^0 decay mode can be used in this analysis if it has a reasonable

Experiment	Charm mass (GeV/c^2)
JADE [78].	1.5
TPC/Two-Gamma [79]	1.6
TASSO [84]	1.6
TOPAZ D* [83]	1.3-1.8, $\mu = m/2$ - $2m$
TOPAZ π_s [80]	1.3; iteratively tuned to the data
TOPAZ lepton [88]	1.3-1.5 (1.6 in fragmentation)
AMY π_s [87]	1.6, $\mu = \sqrt{2}m$
AMY lepton [87]	1.6, $\mu = \sqrt{2}m$
VENUS [89]	Direct 1.6 ± 0.2, Resolved 1.35 ± 0.2 (included in systematic error)
ALEPH [85]	1.6

Table 3: *Treatment of charm mass (m) in extracting experimental results. μ is the renormalisation scale; unless otherwise stated it is equal to the charm mass.*

branching ratio (at least of order 1%). Published results have included the decays $K^-\pi^+$, $K^-\pi^+\pi^0$, $K^-\pi^+\pi^+\pi^-$. Having formed a candidate D^0 meson, which is within the accepted mass range, tracks identified as pions are added in turn to form candidate D^{*+} mesons, ΔM being determined in each case. For background tracks the spectrum rises from a kinematic lower limit of 139.6 MeV/c^2 (M_{π^+}), whilst the signal produces a peak at 145.5 MeV/c^2, i.e. $M_{D^{*+}} - M_{D^0}$, which is a region where the background is small.

Early measurements were reported by JADE [78], TPC/Two-Gamma [79], and TASSO [84]. More recently results have also been produced by TOPAZ [83] and ALEPH [85]. These results are summarised in Table 6. The adjusted figure in column 4 takes account of various factors. For TPC/Two-Gamma [79], JADE [78], TASSO [84] and the earlier TOPAZ result [83], the adjustment accounts for the latest values for the D^{*+} and D^0 branching ratios [86]. The

Electron Energy	Direct (Born term)	Direct (NLO)	Resolved (NLO)
15	75 ± 14	103 ± 19	17 ± 6
17	87 ± 16	120 ± 22	23 ± 8
29	146 ± 26	200 ± 35	70 ± 22
45	206 ± 34	258 ± 36	195 ± 86
80	302 ± 49	416 ± 74	367 ± 120
90	324 ± 53	444 ± 77	440 ± 152

Table 4: *Cross Section (pb) for charm production in two photon physics based on Ref. [74]. The highest values come from using a charm quark mass of* $1.3\,\mathrm{GeV/c^2}$ *with the scale equal to the charm mass. The lowest values use a charm mass of* $1.7\,\mathrm{GeV/c^2}$ *with the scale equal to* $\sqrt{2}$ *times the charm mass. The GRV [11] set of parton densities was used, and a lower cut of 3.8 GeV was applied for the invariant mass of the* $\gamma\gamma$ *system.*

Method	Experiments	N for 500 pb^{-1}	Comments
$D^{*\pm} \to D^0\pi^\pm$	TPC/2γ, TASSO, JADE, TOPAZ AMY, ALEPH	500	clean($\uparrow$), no VMD contribution($\uparrow$), $p_t^{D^*}$ cut($\downarrow$)
Slow pions	TOPAZ, AMY	$\mathcal{O}(10^3)$	large background ($\downarrow$)
$K_s^0 \to \pi^+\pi^-$ ($e_c^4 : e_s^4 = 16$)	TOPAZ	$\mathcal{O}(10^4)$	VMD contribution($\downarrow$) & fragmentation ($\downarrow$), s-quarks ($\downarrow$)
Lepton Tags	TOPAZ, AMY VENUS	$\mathcal{O}(10^2)$	background($\downarrow$), fake leptons($\downarrow$)
Secondary Vertices		?	no b quarks($\uparrow$) boost ?

Table 5: *Summary of experimental methods for tagging charm in $\gamma\gamma$ physics. In column 1 are listed the experiments which have published results in each category. Column 3 is an estimate of the number of events likely to be observed at LEP2 assuming similar selection efficiencies to those at current experiments. Column 3 indicates advantages* ($\uparrow$) *and disadvantages* ($\downarrow$) *of the different techniques.*

published TOPAZ cross section is with the additional condition $p_t^{D^{*+}} > 1.6\,\mathrm{GeV/c}$. A total cross section was obtained from the published figures by multiplying the total QPM cross section by the ratio of the observed cross section to the QPM cross section for the same acceptance.

The *soft pion method* is similar to the D^* tagging method in that it takes advantage of the small kinetic energy available to the soft pion in the decay of a D^* to a D^0, but avoids the reduction of statistics which results in looking for fully reconstructed D^*. It has been found that if one plots the transverse momentum of all charged tracks in events with respect to the jet direction that there is a small excess at very low values which is ascribed to these soft pions. This excess sits on top of a background which is normally estimated by a fit to the p_t distribution in the nearby bins and by Monte Carlo studies. Measurements of this type have been made by TOPAZ [80], and AMY [87] and are summarized in Table 6. Note that TOPAZ published their result for the restricted acceptance $p_t^{D^{*+}} > 1.6\,\mathrm{GeV/c}$, $|\cos(\theta)| < 0.77$.

In the *lepton tagging* technique one uses the fact that there is roughly a 10% branching fraction for a charmed meson decay to include electrons or muons. However the problem is that there are plenty of other sources of leptons in $\gamma\gamma$ events, so a measurement requires good modelling of the background. Results have been published by TOPAZ [88], VENUS [89], and AMY [87] and are summarised in Table 6.

Furthermore, *kaons* may be used for charm tagging; due to the quark charge, and neglecting quark masses, direct strange quark production is suppressed by a factor 16 compared to direct charm quark production in $\gamma\gamma$ collisions. Therefore a large fraction of the K_s observed come from decays of primary charm quarks. However, a substantial number of kaons is also produced

Experiment	Beam energy (GeV)	Published Measurement	$\sigma(e^+e^- \to e^+e^- c\bar{c}\mathrm{X})$ (pb)
TPC/Two-Gamma [79]	14.5	74 ± 32 pb	120 ± 52
JADE [78]	17	20.5 events	365 ± 150
TASSO [84]	17	97 ± 29 pb	142 ± 42
TOPAZ [83]	29	77 ± 25 pb	430 ± 140
ALEPH [85]	45	155 ± 39 pb	326 ± 87
TOPAZ [80]	29	23.5 ± 4.6 pb	304 ± 60
AMY [87]	29	169 ± 48 pb	355 ± 106
Venus [89]	29	68.4 ± 13 events	340 ± 65
TOPAZ [88]	29	19.3 ± 3.4 pb	451 ± 80
AMY [87]	29	1.0 ± 0.23 pb	374 ± 86

Table 6: *Measurements of charm production in two photon physics. The third column shows the published measurement, either number of events or cross section. As these numbers are not directly comparable we have extrapolated them to a total charm cross section in the fourth column. The upper 7 measurements are of* D^{*+} *production, and out of these the first 5 measurement listed employed the 'D* Trick', while the measurements in rows 6 and 7 used the 'Soft Pion' method. The remaining 3 rows report measurements where lepton tagging was employed.*

from strange quarks in soft VMD process and from u, d quarks in the fragmentation. Modelling such production introduces systematic errors. The statistical errors, however, are expected to be very small due to the large number of reconstructed K's. In Fig. 29 the transverse momentum p_t with respect to the beam axis is plotted for K_s from $\gamma\gamma$ collisions reconstructed in a typical LEP detector for $E_{\mathrm{CM}} = 91$ GeV. The events were simulated with PYTHIA 5.7 [41] including the VMD, anomalous and direct photon components. At $p_t(K_s) > 1$ GeV/c the production from primary s and c quarks dominates over the production from u, d quarks. This effect will be even more pronounced at higher energies. The still strong presence of primary s quarks makes the measurement quite dependent on how this contribution is modeled. The only published measurement of K_s production in $\gamma\gamma$ events to date is by TOPAZ [90].

In principle it might be possible to observe the finite decay length of a charm quark using techniques such as those used so succesfully to tag bottom quarks at LEP1 . These techniques take advantage of the vertex detectors installed on LEP detectors and include impact parameter, secondary vertex finding and neural nets. At present none of these techniques has been studied in detail.

7.3 Prospects for LEP2

The cross section for charm production in both the direct and single resolved mode grows with energy. The cross sections at Petra, Tristan, LEP1, and LEP2 energies are shown in Table 4. Using these cross sections with the 500 pb^{-1} promised for LEP2 and assuming that selection

efficiencies will be similar to those at present experiments produces the estimated events rates given in column 3 of Table 5. Note that the total number of $c\bar{c}$ events at LEP2 will be around $5 \cdot 10^5$. It is clear that at LEP2 there is the prospect for high statistics measurements of charm production. With these statistics it should be possible to produce a clean measurement of the resolved and direct processes separately. Recently the direct and resolved contributions to charm production were measured [90] by identifying the energy from the remnant jet, present in resolved processes, seen close to the beam pipe. There is good reason to believe that LEP experiments will be at least as capable of observing this energy and thus extend these studies to higher energies where the contribution of resolved processes is larger. As mentioned in the theory section there is also particular interest in measuring charm production in $\gamma^*\gamma$ events, i.e. in events with a tagged electron. The rates for this will be roughly 5-10% of the untagged rates given in Table 5.

8 Exclusive channels [12]

The formation of light resonances by two-photon interactions is a powerful tool in understanding the hadron spectrum and the dynamics controlling the interaction of their constituents. A rigorous testing ground for nonperturbative QCD is provided by analyses of heavy quarkonia for which relativistic corrections and dynamical effects of gluons can be included in a systematic way. Similarly, the meson-photon transition form-factor at large Q^2 and exclusive (meson and/or baryon) pair production at large p_T can reliably be calculated in QCD. Last but not least, high-energy $\gamma^\star(Q^2)+\gamma \to V_1+V_2$ and/or V_1+X_2 reactions, where either Q^2, the resonance mass or the momentum transfer is large, allow us to enter a new domain of perturbative QCD. Prospects for LEP2 will be discussed in the following.

8.1 Resonance production by quasi-real photons

Two-photon couplings provide a useful probe of the internal structure of mesons. Two quasi-real photons couple in a selective way to $C = +1$ states, thus simplifing the analysis of mass spectra where many hadrons are superimposed. The accessible resonances with spin ≤ 2 have $J^{PC} = 0^{-+}$ ($^1S_0$), 2^{-+} ($^1D_2$), 0^{++} ($^3P_0$), and 2^{++} ($^3P_2$) where we have given in parentheses the $q\bar{q}$ quark-model assignements in the spectroscopic notation. In particular the "classical" resonances have been observed at e^+e^- machines with $\gamma\gamma$ partial widths consistent with quark-model predictions [91]. These are the light pseudoscalar 0^{-+} and tensor 2^{++} states π^0, η, η', $f_2(1270)$, $a_2(1320)$, $f_2'(1525)$, and, although with poor statistics, the $c\bar{c}$ states η_c, χ_{c0}, and χ_{c2}.

Particularly interesting are, of course, those resonances whose $\gamma\gamma$ couplings are not consistent with quark-model estimates. On the one hand, conventional $\gamma\gamma$-width calculations might not be reliable enough. As an example let us mention the $\pi_2(1670)$, thought to be the $^1D_2$ $(u\bar{u} - d\bar{d})/\sqrt{2}$ quarkonium state. Here the discrepancy between the measured $\gamma\gamma$ partial width

[12] A. Buijs, E. Boudinov, W. Da Silva, S.R. Hou, M.N. Kienzle, P. Kroll, J. Parisi, T. van Rhee, G.A. Schuler, B. Wilkens

and the non-relativistic calculation [92] could be due to large relativistic corrections [93]. On the other hand, mesons thought to be non-$q\bar{q}$ states generally have $\gamma\gamma$ widths far from expectations for a $q\bar{q}$ state. These anomalous states include the $f_0(1500)$, $f_{0/2}(1720)$, $f_J(2230)$, the $\eta(1410)$, $\eta(1460)$, and the $f_1(1420)$ (for a recent review see e.g. [94]). Measurements of their $\gamma\gamma$ widths have the potential to resolve the enigma of these mesons.

Exploring the exclusive channels at LEP2 has pros and cons compared to lower-energy machines. There are two advantages. First, the signal cross section $\sigma(\mathrm{e^+e^-} \to \mathrm{e^+e^-R})$ rises[13] with

Experiment	$\sqrt{s}$ (GeV)	$\int L\mathrm{dt}$ pb^{-1}	σ (pb)	A	$\sigma\cdot$A (pb)
CLEO II [100]	11	3000	17	0.54	9.2
TPC/2γ [98]	29	69	48	0.35	16.8
PLUTO [97]	35	45	56	0.33	18.5
L3 [101]	91	30	104	0.25	26.0
LEP2	175	500	147	0.21	30.2

Table 7: *Comparison of existing data samples for $\sigma(\mathrm{e^+e^-} \to \mathrm{e^+e^-}\eta_c)$ with estimates for LEP2. The geometrical acceptance A is defined in the text. The fourth column gives the full resonance production cross-section calculated with exact kinematics and a J/ψ form factor.*

the e^+e^- centre of mass (cm) energy $\sqrt{s}$, while the background from the s-channel annihilation reaction decreases as $\approx 1/s$. Second, since the energy released in annihilation events rises with $\sqrt{s}$, the two contributions become more separated at higher energy [96].

There are also two disadvantages compared to experiments at lower energies. First, the detector acceptance is reduced since the photon-photon system receives on average a larger Lorentz boost. Table 7 displays the acceptance as a function of $\sqrt{s}$ for the case of η_c production [97–102] in the decay channel $\eta_c \to 4\pi$. All LEP detectors have a good solid angle coverage. For our studies we [103] use the following geometrical acceptance: $20^\circ \leq \theta \leq 160^\circ$ for tracks with a $p_t \geq 0.1\,\mathrm{GeV}$ and $15^\circ \leq \theta \leq 165^\circ$ for photons with $\mathrm{E} \geq 0.1\,\mathrm{GeV}$. As can be seen from Table 7 the acceptance slowly decreases with the centre of mass energy. Due to the increase in the cross section, we find still a net gain on the number of observed events. For lighter resonances the acceptance decreases, from $\sim 20\%$ at 3 GeV to $\sim 4\%$ at 1.3 GeV.

The second disadvantage concerns the triggers. Their efficiencies are more difficult to evaluate. Since the interest of the LEP experiments is centered on the maximum available energy, the two-photon events are mainly seen by triggers based on tracks, thus excluding the observation of purely neutral decays of resonances. The combined effect of the trigger and analysis cuts reduces the efficiency by factors varying from about two at a mass of 3 GeV to about 15 at 1.3 GeV. As examples we show in Table 8 the expectations for the lightest 0^{-+} and 2^{++} states. With current triggers, only the η' can be studied in the pseudoscaler octet. The expected rates

[13] In the Low approximation, the two-photon cross-section rises as $\ln^3 s$ for a 4π detector and as $\ln^2 s$ for a realistic, limited angular acceptance detector [95]; compare with Table 7.

Resonance	decay	cross sections (pb)	A	ϵ_{untag}	Events untagged	ϵ_{tag}	Events tagged
π^0		no trigger					
η	$\pi^+\pi^-\pi^0$	no acceptance					
$\eta^{'}$	$\pi^+\pi^-\gamma$	3381±23	0.133	0.0188	9534	0.0016	811
	$\pi^+\pi^-\eta$		0.025	$\leq 10^{-4}$			
f_2	$\pi^+\pi^-$	4463 ± 44	0.264	0.125	159000	0.003	3815
a_2	$\pi^+\pi^-\pi^0$	1436 ± 5.5	0.0416	0.0033	1658	0.0006	301
$f_2^{'}$	K_sK_s	82.04 ± 0.37	0.0935	0.0564	190	0.0011	4

Table 8: *Examples of low-mass resonances at LEP2 ($e^+e^- \to e^+e^-R$ at $\sqrt{s} = 175\ GeV$ for $\mathcal{L} = 500\,pb^{-1}$). A is the geometrical acceptance as described in the text and ϵ the efficiency including trigger and analysis cuts: ϵ_{untag} for untagged and ϵ_{tag} for tagged events ($0.2 \leq Q^2 \leq 0.8\ GeV^2$, and $Q^2 \geq 7\ GeV^2$). The third column gives the full resonance production cross-section, while the number of events is calculated taking into account the branching ratio.*

for the tensor octet are rather good, an analysis of these data has already started at LEP1 [104].

Let us emphasize the generally very low efficiencies, for example, the a_2 in Table 8. Its trigger could easily be improved to reach the acceptance limit [103]. We conclude that, if specialized triggers are installed, good results on light resonance physics can be achieved except for purely neutral decays. Hence even searches for glueballs might be within reach. Since their two-photon widths are expected to be at least one order of magnitude below that of normal $q\bar{q}$ states [105, 106], searches for associated glueball (G) production, $\gamma\gamma \to \pi^0 G$ are welcome: of the order of 10 to 100 events should be produced above $p_T = 1\,\mathrm{GeV}$ at $500\,\mathrm{pb}^{-1}$ [107].

8.2 Resonance production with one off-shell photon

Resonances can also be studied in two-photon events in which one photon is far off the mass shell. Usually, this is the domain of single-tag events where the virtuality Q^2 is determined from a measurement of the scattered electron. The Q^2 range can be extended by including no-tag events, in which case Q^2 is reconstructed by the measurement of the p_T of the resonance. In particular one may cover Q^2 ranges where the Q^2 determination from the electron is not possible (i.e. from about $0.8\,\mathrm{GeV}^2$ to $7\,\mathrm{GeV}^2$ at LEP2). Note that resonance production in single-tag events is just the exclusive limit of the photon structure function (i.e. $e\gamma \to eM$). The interest here is twofold. First, the meson–photon transition form factor can be measured, and secondly, spin-1 states can be produced (the Landau–Yang theorem forbids their production from two on-shell photons). Measurements of the pseudoscalar–photon transition form factors are now becoming quite precise [108]. Also the 1^{++} ($^3P_1\ q\bar{q}$) state $f_1(1285)$ has been observed [109] with a $\gamma\gamma$ coupling consistent with quark-model estimates [110] for $Q^2 \neq 0$ photons.

The LEP experiments can cover a large Q^2 range with various tagging systems, *e.g.* for L3:

VSAT (very small angle tagger) ($0.2 \leq Q^2 \leq 0.8\,\mathrm{GeV}^2$), LUMI (luminosity monitor) ($Q^2 \geq 7\,\mathrm{GeV}^2$), and ECAL (the endcap electromagnetic calorimeter) ($Q^2 \geq 40\,\mathrm{GeV}^2$). Given the high cm energy, high Q^2 values should be reachable. We estimate that form-factor measurements will, even with current triggers, be possible for at least the η', the f_2, and the η_c, see Table 8 and Fig. 30. Concerning the spin-1 mesons, the f_1 and χ_{c1} will certainly be observed. Otherwise

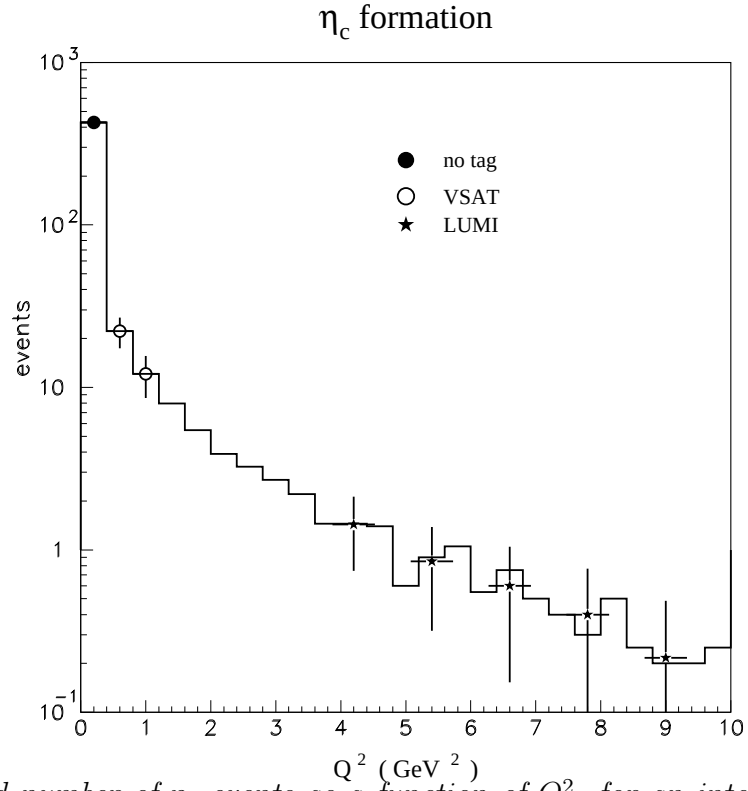

Figure 30: *Expected number of η_c events as a function of Q^2, for an integrated luminosity of 500 pb^{-1}. All observable decay channels are included.*

the same remark as above applies: with more dedicated triggers more resonances will become accessible.

Theoretical predictions for the η_c-photon transition form factor $F_{\eta_c\gamma}(Q^2)$ [111] are shown in Fig. 31, as well as a similar calculation [112] for $F_{\pi\gamma}(Q^2)$ compared to recent data [108, 113]. For low Q^2, models based on vector-meson-dominance (VMD), constituent quarks, QCD sum rules or chiral perturbation theory work, in general, successfully for pseudoscalar mesons (P), see e.g. ref. [114]. The Q^2 dependence can be parametrized by

$$F_{P\gamma}(Q^2) = \frac{A_P}{1 + Q^2/\Lambda_P^2} \; . \tag{30}$$

For example, in VMD A_P is related to the $V\pi\gamma$ and Ve^+e^- coupling constants (here V is the corresponding vector state(s), i.e. ρ and ω for the π^0, and J/ψ for the η_c), and Λ_P is given by the vector-meson mass.

Form factors are particularly interesting at high Q^2 since a factorization formula holds [115],

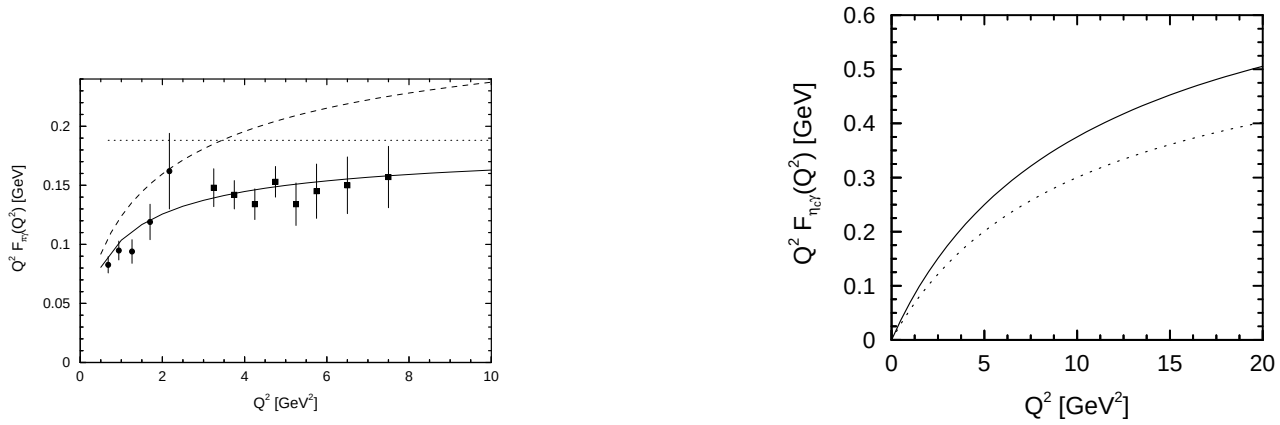

Figure 31: *Left: The $\pi\gamma$ transition form factor vs. Q^2. The solid (dashed) line represents the prediction obtained with the modified HSA using the asymptotic (CZ) wave function [112]. The dotted line represents the results of the standard HSA for the asymptotic wave function. Data are taken from [113], [108]. Right: The $\eta_c\gamma$ transition form factor calculated assuming for the η_c decay constant 383 MeV (solid line) and 284 MeV (dotted line).*

which expresses large-Q^2 exclusive reactions as a product of process-independent meson distribution amplitudes and perturbatively calculable short-distance coefficients. In fact, asymptotically, i.e. for $\ln Q^2/\mu_0^2 \to \infty$ (μ_0 a typical hadronic scale $\sim$ 0.5–1 GeV), the distribution amplitudes are known and one derives the parameter-free result [115, 116]

$$F_{P\gamma}(Q^2) \to \frac{\sqrt{2} f_P}{Q^2} \tag{31}$$

where f_P is the meson's decay constant (i.e. 130.7 MeV for the pion). A simple all-Q^2 formula is arrived at [115] by assuming (30) and fixing the two parameters from (31) ($\Lambda_P = 2\pi f_P$) and the PCAC value of the form factor at $Q^2 = 0$ ($A_P = 1/(2\sqrt{2}\pi^2 f_P)$).

For finite Q^2, a comparison of the full calculation and data allows the determination of the distribution amplitude. The calculations shown in Fig. 31 are based on a modified hard-scattering-approach (HSA) to exclusive reactions, in which transverse degrees of freedom, representing higher twist effects, and Sudakov suppression are taken into account. The pion data nicely agree with the calculation if one uses a wave function $\sim \exp[-a^2 k_\perp^2/x(1-x)]$, which leads, after $k_\perp$-integration, to the asymptotic distribution amplitude $\sim x(1-x)$ (x is the momentum fraction carried by the quark inside the pion). In contrast, the use of a wave function implying the Chernyak-Zhitnitsky distribution amplitude [117], leads to results in severe conflict with the data, see Fig. 31. That observation may have far-reaching consequences for our understanding of other large momentum transfer exclusive reactions, as for instance $\gamma\gamma \to \pi\pi$.

The η_c-photon transition form factor has not yet been measured. The predictions shown in Fig. 31 are obtained using the Bauer-Stech-Wirbel wave function [118]

$$\Psi_0(x, \mathbf{k}_\perp) = N x(1-x) \exp\left[-a^2 M_{\eta_c}^2 (x-1/2)^2\right] \exp\left[-a^2 k_\perp^2\right] \ . \tag{32}$$

Its two parameters, namely the transverse size parameter a and the normalization constant N cannot be fully fixed from the $\eta_c \to \gamma\gamma$ decay width. To illustrate the parameter dependence we

have taken the valence quark Fock state probability to be 0.8 and required a value of either 383 MeV or 284 MeV for the η_c decay constant. Referring to Fig. 30, a measurement of $F_{\eta_c\gamma}(Q^2)$ up to $Q^2 \sim 10\,\mathrm{GeV}^2$ seems feasible.

8.3 Charmonium

The heavy quark systems can, to first approximation, be described by nonrelativistic quark-potential models and many of their properties are expected to reflect the underlying dynamics of QCD. For example (see e.g. [119]),

$$\Gamma(\eta_c \to \gamma\gamma) = \frac{64\pi\alpha^2}{27M_c^2}|\Psi_{\eta_c}(0)|^2\left[1 - \frac{3.4}{\pi}\alpha_s(M_c)\right] \ . \tag{33}$$

Here $\Psi_{\eta_c}(0)$, the non relativistic wave function at the origin, contains all non-perturbative QCD effects. Replacing the two photons by two gluons gives $\Gamma(\eta_c \to gg)$ which, in the potential model, is the total width Γ_{η_c} of the η_c. It turns out [120] that the value of $\alpha_s(M_c)$ determined from the relation,

$$\frac{\Gamma_{\eta_c}}{\Gamma(\eta_c \to \gamma\gamma)} = \frac{9\alpha_s(M_c)^2}{8\alpha^2}\left[1 + \frac{8.2}{\pi}\alpha_s(M_c)\right] \tag{34}$$

is about 3 standard deviations below the value expected from other QCD measurements: $\alpha_s(M_c) = 0.33 \pm 0.02$ [96]. This indicates that corrections to the non-relativistic quark-potential model are non-negligible. Recently, a rigorous factorization of heavy quarkonium decays has been developed [121, 122]. Both relativistic corrections and effects of dynamical gluons (those associated with the binding) can be calculated in a systematic way. Phenomenological studies [120, 123, 124] show results that depend crucially on the input data.

These problems can be solved by high precision LEP measurements of the two-photon widths $\Gamma_{\gamma\gamma}$ for charmonium states. In Table 9 we estimate the expected number of events for the charmonium states decaying into 4π. For tagged events, the Q^2 dependence is modelled by a J/ψ form-factor. Since the charmonia have very small branching ratios into 4π [86], the

Resonance	cross sections (pb)	A	ϵ_{untag}	Events untagged	ϵ_{tag}	Events tagged
η_c	146.8±1.5	0.21	0.11	97	0.01	9.
χ_{c0}	25.9±0.3	0.22	0.12	57	0.01	6.
χ_{c2}	18.2±0.11	0.22	0.12	17.5	0.01	2.

Table 9: *Example of charmonium production expected at LEP2; given is the channel* $e^+e^- \to e^+e^-R$, $R \to 4\pi$ *for* $\mathcal{L} = 500\,pb^{-1}$ *at* $\sqrt{s} = 175\,GeV$. *A and* ϵ *as in Table 8.*

number of events can be increased substantially (factors 5–6) by measuring also other decay channels [101, 103]. Hence good measurements of the charmonium states, including the χ_{c1} are expected.

8.4 Exclusive pair production

Two-photon exclusive meson and baryon production provides particularly clean tests of QCD. At large angles, a factorization holds [115] which tells us that the exclusive scattering amplitude is given as the product of a hard scattering amplitude and soft distribution amplitudes $\Phi_i(x, p_T^2)$. Although the latter are nonperturbative quantities, they are subjected to several constraints (evolution equation in p_T, asymptotic ($p_T \to \infty$) form, normalization in the case of mesons). This leads to a parameter-independent prediction for the fall-off with $s_{\gamma\gamma}$ at fixed angle ($d\sigma/dt \propto s_{\gamma\gamma}^{-4}$, $s_{\gamma\gamma}^{-6}$ for meson and baryons, respectively) and essentially parameter-independent predictions for the angular distribution at moderate $s_{\gamma\gamma}$ (see e.g. [3]). Current experiments reach $\sqrt{s_{\gamma\gamma}}$ values up to about 3 GeV, where a transition from the VMD-like angular distribution to the one predicted by the HSA just becomes visible. Production of pseudoscalar- and vector-meson pairs at LEP2 has been estimated during the last workshop: sufficient counting rates can be expected to test the predictions up to $\sqrt{s_{\gamma\gamma}} \approx$5–6 GeV [3].

Calculations within the HSA have been extended in various ways. On the one hand, the potentially dangerous endpoint regions in the x integration have been shown to be suppressed by Sudakov form factors [125]. On the other hand, predictions now exist for the pair production of baryons [126], heavy mesons (D, $D^\star$) [127], and (light) mesons with non-zero orbital angular momenta [128]. Among the $L > 0$ mesons, $a_2^+ a_2^-$ might have a rate large enough to be observable at LEP2, namely about 500 (50) events for a p_T-cut of 1 GeV (2 GeV) (without taking into account experimental cuts).

The standard (or possibly improved) HSA gives the leading-twist cross section at fixed cm scattering angle or, equivalently, at fixed $t/s_{\gamma\gamma}$. At LEP2, a new domain of perturbative QCD may be entered. This is the region $\mu_0^2 \ll |t| \ll s_{\gamma\gamma}$ (so-called semi-hard region) which is discussed in sec. 5 where numerical estimates are presented.

8.5 Summary

In summary, many light resonances can be studied with good counting rates at LEP2, provided the triggers of the experiments will be extended to low-momentum charged particles. The trigger efficiency and acceptance generally increases with the resonance mass. Good results can be expected for the four lowest-lying $C = +1$ charmonium states. Bottomonium resonances, however, are beyond the reach of LEP2. Measurements of spin-1 mesons (notably the f_1 and the χ_{c1}) and various meson–photon transition form factors will be possible both in single-tag events and in untagged events through Q^2 reconstruction from the hadronic final state. Measurements of conventional pair production of S-wave mesons should be possible up to 5–6 GeV CM energy, allowing for definite tests of the HSA. Effects of QCD in a new perturbative domain are expected to become accessible in semi-hard reactions.

Acknowledgements: We warmly thank J. Butterworth (ZEUS), M. Erdmann (H1), and H. Hayashii (TOPAZ) for interesting discussions about recent HERA and TRISTAN results.

References

[1] H. Kolanoski and P. Zerwas in High Energy Electron-Positron Colliders, A. Ali and P. Söding *eds.*, World Scientific, Singapore, 1988.

[2] M. Drees and R.M. Godbole, hep-ph/9508221, University Wisconsin preprint MAD-PH-898, July 1995, to appear in J. of Physics **G**.

[3] D.J. Miller et al., Proceedings of the Workshop on LEP200 Physics, Aachen, 1986, p. 202.

[4] Report on the $\gamma\gamma$ Event Generators working group, these proceedings.

[5] For recent reviews on photon structure, see e.g.
H. Abramowicz et al., Int. J. Mod. Phys. **A8** (1993) 1005; see also [1, 2].

[6] OPAL Collab., R. Akers et al., Z. Phys. **C61** (1994) 199;
DELPHI Collab., P. Abreu et al., CERN PPE/95-87.

[7] PLUTO Collab., Ch. Berger et al., Phys. Lett. **B142** (1984) 111; *Nucl. Phys.* **B281** (1987) 365;
JADE Collab., W. Bartel et al., Z. Phys. **C24** (1984) 231;
TASSO Collab., M. Althoff et al., Z. Phys. **C31** (1986) 527;
TPC/2γ Collab., H. Aihara et al., Phys. Rev. Lett. **58** (1987) 97; Z. Phys. **C34** (1987) 1;
AMY Collab., T. Sasaki et al., Phys. Lett. **B252** (1990) 491, S.K. Sahu et al., Phys. Lett. **B346** (1995) 208;
TOPAZ Collab., K. Muramatsu et al., Phys. Lett. **B332** (1994) 477.

[8] ZEUS Collab., M. Derrick et al., Phys. Lett. **B316** (1993) 412, Z. Phys. **C65** (1995) 379;
H1 Collab., I. Abt et al., Nucl. Phys. **B407** (1993) 515; T. Ahmed et al., Nucl. Phys. **B439** (1995) 471.

[9] PLUTO Collab., Ch. Berger et al., Phys. Lett. **142B** (1984) 119.

[10] C.F. Weizsäcker, Z. Phys. **88** (1934) 612; E.J. Williams, Phys. Rev. **45** (1934) 729.

[11] M. Glück, E. Reya and A. Vogt, Phys. Rev. **D46** (1992) 1973.

[12] V.S. Fadin, E.A. Kuraev, L.N. Lipatov, Sov. Phys. JETP **45** 262 (1977) 199,
Y.Y. Balitsky, L.N. Lipatov, Sov. J. Nucl. Phys. **28** (1978) 822.

[13] M. Glück, E. Reya and A. Vogt, Z. Phys. **C53** (1992) 127, Phys. Lett. **B306** (1993) 391, Z. Phys. **C67** (1995) 433.

[14] R.D. Ball and S. Forte, Phys. Lett. **B335** (1994) 77, **B336** (1994) 77.

[15] F.A. Berends, P.H. Daverveldt and R. Kleiss, Nucl. Phys. **B253** (1985) 421; Comput. Phys. Comm. **40** (1986) 271.

[16] E. Laenen and G.A. Schuler, CERN-TH/95-233.

[17] E. Laenen, S. Riemersma, J. Smith and W.L. van Neerven, Phys. Rev. **D49** (1994) 5753.

[18] M. Glück, E. Reya and A. Vogt, Phys. Rev. **D45** (1992) 3986, **D48** (1993) 116.

[19] P. Aurenche, M. Fontannaz and J.P. Guillet, Z. Phys. **C64** (1994) 621.

[20] A. Vogt, Proceedings of the Workshop on Two-Photon Physics at LEP and HERA, Lund, May 1994, eds. G. Jarlskog and L. Jönsson (Lund Univ., 1994), p. 141.

[21] C. Peterson, T.F. Walsh and P.M. Zerwas, Nucl. Phys. **B229** (1983) 301; J.H. Field, F. Kapusta and L. Poggioli, Phys. Lett. **181B** (1986) 362, Z. Phys. **C36** (1987) 121.

[22] TASSO Collab., M.Althoff et al., Phys. Lett. **138B** (1984) 219;
PLUTO Collab., Ch.Berger et al., Z. Phys. **C26** (1984) 191, **C29** (1985) 225, **C33** (1987) 351.

[23] G.A. Schuler and T. Sjöstrand, Z. Phys. **C68** (1995) 607.

[24] V. Blobel, Proceedings of CERN school of computing, Aiguablava, Spain, September 1984, ed C. Verkerk.

[25] W.R. Frazer, Phys. Lett. **B194** (1987) 287.

[26] P. Kessler, 10th Workshop on Photon-photon Collisions (PHOTON'95), Sheffield, U.K, April 1995, B. Cartwright, D.J. Miller and V.A. Khoze *eds*;
J.H. Field, UGVA-DPNC-1995-6-165, *ibid.*

[27] F. Le Diberder (CELLO Collab.), in "Seminar on $\gamma\gamma$ Physics", Paris 1984, ed. J.H. Field, preprint LPNHE Paris 84-05.

[28] C. Jacobsson, Lund University PhD thesis, 1994.

[29] CELLO Collab., Phys. Lett. **B126** (1983) 384.

[30] E. Leonardi, talk presented at PHOTON'95, Sheffield, U.K., April 1995, B. Cartwright, D.J. Miller and V.A. Khoze *eds*.

[31] G. Marchesini et al., Comput. Phys. Comm. **67** (1992) 465;
L. Lönnblad and M.H. Seymour, these proceedings.

[32] S. Catani, Y.L. Dokshitzer and B.R. Webber, Phys. Lett. **B285** (1992) 291.

[33] M.H. Seymour, Nucl. Phys. **B436** (1995) 443.

[34] F.M. Borzumati and G.A. Schuler, Z. Phys. **C58** (1993) 139;
M. Drees and R.M. Godbole, Phys. Rev. **D50** (1994) 3124.

[35] P. Aurenche, J.-Ph. Guillet, M. Fontannaz, Y. Shimizu, J. Fujimoto and K. Kato, Prog. Theor. Phys. **92** (1994) 175.

[36] M. Glück, E. Reya and M. Stratmann, Phys. Rev. **D51** (1995) 3220.

[37] T. Uematsu and T.F. Walsh, Phys. Lett. **B101** (1981) 263, Nucl. Phys. **B199** (1982) 93;
G. Rossi, Univ. California report UCSD-10P10-227 (1983), Phys. Rev. **D29** (1984) 852.

[38] ZEUS collaboration, M. Utley, presented at the EPS Conference, Brussels, 1995.

[39] V.M. Budnev et al., Phys. Rep. **15** (1975) 181;
P. Kessler, Proceedings of the Workshop on Two-Photon Physics at LEP and HERA, Lund, May 1994, G. Jarlskog and L. Jönsson *eds*.

[40] J.H. Field, Nucl. Phys. **B168** (1980) 477, **B176** (1980) 545;
Ch. Berger and J.H. Field, Nucl. Phys. **B187** (1981) 585.

[41] T. Sjöstrand, Comput. Phys. Comm. **82** (1994) 74; PYTHIA 5.7 and JETSET 7.4: Physics and manual, preprint CERN-TH.7112/93-REV

[42] H1 Collab.: S. Aid et al., DESY 95-156, 1995.

[43] H1 Collab., I. Abt et al., Phys. Lett. **B328** (1994) 176.

[44] G.A. Schuler, in "Proc. of the Workshop on Two-Photon Physics at LEP and HERA", Lund, May 1994, G. Jarlskog and L. Jönsson *eds*., p. 200.

[45] G.A. Schuler and T. Sjöstrand, Phys. Rev. **D49** (1994) 2257.

[46] A. Capella et al., Phys. Rep. **236** (1994) 227.

[47] R. Engel, Z. Phys. **C66** (1995) 203.

[48] R. Engel and J. Ranft, ENSLAPP-A-540/95 (hep-ph/9509373), 1995.

[49] J.M. Butterworth and J.R. Forshaw, J. Phys. **G19** (1993) 1657;
J.M. Butterworth, J.R. Forshaw and M.H. Seymour, CERN-TH/95-82, in preparation.

[50] G.A. Schuler and T. Sjöstrand, Phys. Lett. **B300** (1993) 169.

[51] G.A. Schuler and T. Sjöstrand, Nucl. Phys. **B407** (1993) 539;
in "Proc. of Workshop on Two Photon Physics from DAΦNE to LEP200 and Beyond", Paris 1994, F. Kapusta and J. Parisi *eds*, World Scientific, Singapore, p. 163.

[52] A. Corsetti, R. Godbole and G. Pancheri, in preparation, 1995.

[53] ZEUS Collab., Phys. Lett. **B354** (1995) 163.

[54] DELPHI Collab., P.Abreu *et al.*, Phys. Lett. **B342** (1995) 402.

[55] TPC-2γ Collab., D.Bintinger *et al.*, Phys. Rev. Lett. **54** (1985) 763.

[56] ALEPH Collab., Phys. Lett. **B313** (1993) 509.

[57] V.L. Chernyak and A.R. Zhitnitsky, Nucl. Phys. **B222** (1983) 382; Phys. Rep. **112** (1984) 173; I.F. Ginzburg, D.Yu. Ivanov, V.G. Serbo. Sov.Yad.Fiz. **56** (1993) 45.

[58] I.F. Ginzburg, S.L. Panfil, V.G. Serbo, Nucl.Phys. **B284** (1987) 685; I.F. Ginzburg, D.Yu. Ivanov, Nucl. Phys. B (Suppl.) **25B** (1992) 224; Nucl.Phys. **B388** (1992) 376.

[59] J.R.Forshaw and M.G.Ryskin, Z.Phys. **C68** (1995) 137.

[60] Ya.Ya. Balitski, L.N. Lipatov. Sov. J. Nucl.Phys. **28** (1978) 822; L.N.Lipatov. Sov. Phys. JETP **63** (1986) 904; in "Perturbative QCD". ed. A.H.Mueller, World Sc., Singapore, (1989) P.Gauron, L.N.Lipatov and B.Nicolescu. Phys. Lett. **B260** (1991) 407.

[61] P. Aurenche, J.-Ph. Guillet, M. Fontannaz, Y. Shimizu, J. Fujimoto and K. Kato, Proceedings of the Workshop on Two-Photon Physics at LEP and HERA, Lund, May 1994, G. Jarlskog and L. Jönsson *eds*.

[62] T. Ahmed, H1 collaboration, Nucl. Phys. **B445** (1995) 195;
M. Derrick, ZEUS collaboration, Phys. Lett. **B348** (1995) 665.

[63] T. Kleinwort and G. Kramer, preprint DESY-95-172.

[64] TOPAZ Collab., H. Hayashii et al., Phys. Lett. **B314** (1993) 149.

[65] AMY Collab., B.J. Kim et al., Phys. Lett. **B325** (1994) 248.

[66] R. Engel and J. Ranft, to be published (1995).

[67] H1 Collab., "Jets and energy flow in γp collisions at HERA", contr. 0476 to the EPS Conference, Brussels 1995;
ZEUS Collab., "Global event properties in photoproduction at HERA", contr. 0380 to the EPS Conference, Brussels 1995.

[68] P. Chiappetta, M. Greco, J.Ph. Guillet, S. Rolli, M. Werlen, Nucl. Phys. **B412** (1994) 3;
M. Greco and S. Rolli, Phys. Rev. **D52** (1995) 3853;
J. Binnewies, B.A. Kniehl and G. Kramer, preprints DESY-95-048, 95-114.

[69] D. Cords et al., Mark II collaboration, Phys. Lett. **B302** (1993) 341.

[70] P. Aurenche, R. Baier, A. Douiri, M. Fontannaz and D. Schiff Z. Phys. **C29** (1985) 423; L.E. Gordon, Phys. Rev. **D50** (1994) 6753.

[71] See *e.g.*: OPAL Collab., Z. Phys. **C68** (1995) 179, 531; L3 Collab., Phys. Lett. **B345** (1995) 74.

[72] V.N. Baier *et al.*, Phys. Rep. **78** (1981) 193.

[73] M. Dubinin, hep-ph/9504366.

[74] M. Drees, M. Krämer, J. Zunft and P.M. Zerwas, Phys. Lett. **B306** (1993) 371;
M. Krämer, proceedings of Photon 95, Sheffield, UK.

[75] M. Krämer and E. Laenen, preprint CERN-TH/95-291, DESY 95-199.

[76] M. Cacciari and M. Greco, B.A. Kniehl, M. Krämer, G. Kramer and M. Spira, DESY 95-205.

[77] B. Mele and P. Nason, Nucl. Phys. **B361** (1991) 626;
M. Cacciari and M. Greco, Nucl. Phys. **B421** (1994) 530.

[78] JADE Collab., W. Bartel et al. , Phys. Lett. **B184** (1987) 288;
A.J. Finch in Proceedings of the VIII International Workshop on Photon-Photon Collisions, Shoresh, Israel (1988), U. Karshon ed. (World Scientific), p. 75;
The selection efficiences were 0.31% for the $K^+\pi^-\pi^0$ channel and 0.27% in the $K^+\pi^-\pi^0\pi^0$ channel (J.M. Nye, private communication).

[79] TPC/Two-Gamma Collab., M. Alston-Garnjost et al. Phys. Lett. **B252** (1990) 499.

[80] TOPAZ Collab., R. Enomoto et al. Phys. Lett. **B328** (1994) 535.

[81] E. Laenen, S. Riemersma, proceedings of Photon 95, Sheffield, UK; CERN-TH-95-324

[82] M. Krämer, J. Zunft, J. Steegborn and P. Zerwas, Phys. Lett. **B348** (1995) 657;
M. Krämer, DESY 95-155.

[83] TOPAZ Collab., R. Enomoto et al. Phys. Rev. **D50** (1994) 1879.

[84] TASSO Collab., W. Braunschweig et al., Z. Phys. **C47** (1990) 499.

[85] ALEPH Collab., D. Buskulic et al., Phys. Lett. **B255** (1995) 595.

[86] L. Montanet et al. (Particle Data Group), Phys. Rev. **D 50**, Part 1 (1994).

[87] T. Nozaki (AMY Collab.), in Proceedings of PHOTON 95, Sheffield (1995), S.Cartwright, D.Miller and V.A. Khose *eds* (World Scientific).

[88] TOPAZ Collab., R. Enomoto et al. Phys. Lett. **B341** (1994) 99.

[89] VENUS Collab., S. Uehara et al. Z.Phys. **C63** (1994) 213.

[90] TOPAZ Collab., R. Enomoto et al. Phys. Lett. **B341** (1994) 341.

[91] Proc. "VIII International Workshop on Photon–Photon Collisions", Shoresh, Israel (1988), ed. U. Karshon, World Scientific, Singapore 1989;
S. Kawabata, in "Joint Int. Lepton–Photon Symposium & Europhysics Conf. on High-Energy Physics", Geneva, Switzerland (1991), eds. S. Hegarty, K. Potter and E. Quercigh, World Scientific, Singapore 1992, p. 51;
Proc. "IX International Workshop on Photon–Photon Collisions", La Jolla (1992), eds. D.O. Caldwell and H.P. Paar, World Scientific, Singapore 1992;
D.J. Miller, in "Lepton Photon Symposium", Cornell, USA (1993), ed. P. Drell;
Proc. "Photon95", Sheffield, England (1995)

[92] J. D. Anderson, M. H. Austern and R. N. Cahn, Phys. Rev. **D41** (1991) 2094

[93] E.S. Ackleh, T. Barnes, Phys. Rev. **D45** (1992) 232

[94] N.A. Törnqvist, "Summary of Gluonium95 and Hadron95 Conferences", Int. Europhysics Conf. on High-Energy Physics, Brussels, 1995, to be published in the Conf. Proc. by World Scientific

[95] A. Courau, in "Two-Photon Physics", Paris, France (1994), World Scientific Singapore, 1994, eds. F. Kapusta and J. Parisi, p. 1

[96] J.H. Field , in "Two-Photon Physics", Paris, France (1994), World Scientific Singapore, 1994, eds. F. Kapusta and J. Parisi, p. 222

[97] PLUTO Collab., Ch.Berger et al., Phys. Lett. **B167** (1986) 120

[98] TPC/2γ Collab., H. Aihara et al., Phys. Rev. Lett. **60** (1988) 2355

[99] TASSO Collab., W. Braunschweig et al., Z. Phys. **C41** (1989) 533

[100] CLEO Collab., W.Y. Chen et al., Phys. Lett. **B234** (1990) 169;
V.Savinov and R.Fulton, contribution to PHOTON 95, Sheffield, England (1995)

[101] L3 Collab., O. Adriani et al., Phys. Lett. **B318** (1993) 575

[102] ARGUS Collab., H. Albrecht et al., Phys. Lett. **B338** (1994) 390

[103] E. Boudinov (DELPHI), A. Buijs, S. Hou, M.N. Kienzle, T. van Rhee, J.H. Field (L3), B. Wilkens (OPAL), "Resonances formation by photon-photon interaction at LEP2", LEP notes in preparation

[104] S.R. Hou, "The $\pi^+\pi^-\pi^0$ resonances in two-photon collisions", L3 Note 1854 (1995);
S. Braccini, "Study of the $K^0_sK^0_s$ final state in two-photon collisions", L3 Note 1737 (1995);
L3 Collab., O. Adriani et al., CERN-PPE/95-118

[105] G.J. Gounaris, J.E. Pascalis, Nucl. Phys. **B346** (1990) 84

[106] E. H. Kada, P. Kessler and J. Parisi, Phys. Rev. **D39** (1989) 2657

[107] A. Ichola and J. Parisi, Z. Phys. **C66** (1995) 653

[108] CLEO Collab., V. Savinov, contribution to PHOTON 95, Sheffield, England (1995)

[109] TPC/2γ Collab., H. Aihara et al., Phys. Rev. **D38** (1988) 1

[110] R. N. Cahn, Phys. Rev. **D35** (1987) 3342

[111] P. Kroll and M. Raulfs, in preparation

[112] R. Jakob, P. Kroll and M. Raulfs, hep-ph/94 10 304, Wuppertal (1994); P. Kroll, contribution to the PHOTON 95 conference, Sheffield (1995)

[113] CELLO Collab., H.-J. Behrend et al., Z. Phys. **C49** (1991) 401

[114] Ll. Ametller, J. Bijnens, A. Bramon and F. Cornet, Phys. Rev. **D45** (1992) 986

[115] G. P. Lepage and S. J. Brodsky, Phys. Rev. **D22**(1980) 2157; Phys. Rev. **D24** (1981) 1808

[116] T. F. Walsh and P. Zerwas, Nucl. Phys. **B41** (1972) 551

[117] V. L. Chernyak and A. R. Zhitnitsky, Nucl. Phys. **B201** (1982) 492

[118] M. Bauer, B. Stech and M. Wirbel, Z. Phys. **C29** (1985) 637

[119] W. Kwong, P.B. Mackenzie, R. Rosenfeld and J.L. Rosner, Phys. Rev. **D37**, 3210 (1988)

[120] M. Consoli and J. H. Field, Phys. Rev. **D49**, 1293 (1994); Univ. of Geneva preprint UGVA-DPNC 1994/12-164

[121] G.T. Bodwin, E. Braten, G.P. Lepage Phys. Rev. **D46** (1992) 1914 , Phys. Rev. **D51** (1995) 1125

[122] T. Mannel, G.A. Schuler, Phys. Lett. **B349** (1995) 181; Z. Phys. **C67** (1995) 159

[123] G.A. Schuler, preprint CERN-TH.7170/94 (1994)

[124] M.L. Mangano, A. Petrelli, Phys. Lett. **B352** (1995) 445

[125] H.N. Li and G. Sterman, Nucl. Phys. **B381** (1992) 129;
T. Gousset and B. Pire, in "Two-Photon Physics", Paris, France (1994), World Scientific Singapore, 1994, eds. F. Kapusta and J. Parisi, p. 114

[126] G.R. Farrar, H. Zhang, A.A. Ogloblin and I.R. Zhitnitsky, Nucl. Phys. **B311** (1989) 585;
P. Kroll et al., Phys. Lett. **B316** (1993) 546

[127] V.V. Kiselev, preprint IHEP 95-8, Protvino 1995

[128] A. Ichola, L. Houra–Yaou, P. Kessler and J. Parisi, in "Two-Photon Physics", Paris, France (1994), World Scientific Singapore, 1994, eds. F. Kapusta and J. Parisi, p. 143